# Muscle-resident mesenchymal progenitors sense and repair peripheral nerve injury via the GDNF-BDNF axis

**Kyusang Yoo[1], Young-Woo Jo[1], Takwon Yoo[1], Sang-Hyeon Hann[1], Inkuk Park[1], Yea-Eun Kim[1], Ye Lynne Kim[1], Joonwoo Rhee[1], In-Wook Song[1], Ji-Hoon Kim[1,2], Daehyun Baek[1] and Young-Yun Kong[1*]**

[1] School of Biological Sciences, Seoul National University, Seoul 08826, Republic of Korea

[2] Molecular Recognition Research Center, Korea Institute of Science and Technology, Seoul 02792, Republic of Korea

[*]Correspondence and requests for materials should be addressed to Y.Y.K. (ykong@snu.ac.kr)

## Author Contributions

Conceptualization, K.Y. and Y.Y.K.; Methodology, K.Y.; Software, K.Y. and T.Y.; Validation, K.Y., Y.W.J., T.Y., D.B. and Y.Y.K.; Formal analysis, K.Y., and Y.W.J.; Investigation, K.Y. and Y.W.J.; Resources, K.Y., Y.W.J., S.H.H., I.P., Y.E.K., J.R., I.W.S. and J.H.K.; Data curation, K.Y.; Writing – original draft, K.Y.; Writing – review & editing, K.Y., Y.W.J., Y.E.K., Y.L.K. and Y.Y.K.; Visualization, K.Y., and Y.W.J.; Supervision, Y.Y.K.; Project administration, Y.Y.K.; Funding acquisition, Y.Y.K..

## Declaration of interests

The authors declare no competing interests.

**Abstract**

Fibro-adipogenic progenitors (FAPs) are muscle-resident mesenchymal progenitors that can contribute to muscle tissue homeostasis and regeneration, as well as postnatal maturation and lifelong maintenance of the neuromuscular system. Recently, traumatic injury to the peripheral nerve was shown to activate FAPs, suggesting that FAPs can respond to nerve injury. However, questions of how FAPs can sense the anatomically distant peripheral nerve injury and whether FAPs can directly contribute to nerve regeneration remained unanswered. Here, utilizing single-cell transcriptomics and mouse models, we discovered that a subset of FAPs expressing GDNF receptors *Ret* and *Gfra1* can respond to peripheral nerve injury by sensing GDNF secreted by Schwann cells. Upon GDNF sensing, this subset becomes activated and expresses *Bdnf*. FAP-specific inactivation of *Bdnf* (*Prrx1*$^{Cre}$; *Bdnf*$^{fl/fl}$) resulted in delayed nerve regeneration owing to defective remyelination, indicating that GDNF-sensing FAPs play an important role in the remyelination process during peripheral nerve regeneration. In aged mice, significantly reduced *Bdnf* expression in FAPs was observed upon nerve injury, suggesting the clinical relevance of FAP-derived BDNF in the age-related delays in nerve regeneration. Collectively, our study revealed the previously unidentified role of FAPs in peripheral nerve regeneration, and the molecular mechanism behind FAPs' response to peripheral nerve injury.

40 **Introduction**

41 Positioned in the interstitial space between myofibers (Uezumi, et al., 2010), fibro-adipogenic
42 progenitors (FAPs) interact with cellular components within skeletal muscle to ensure normal
43 development, homeostasis, and regeneration of muscle tissue. During developmental
44 myogenesis, embryonic FAPs expressing *Osr1* contribute to limb muscle patterning by
45 regulating the expression of extracellular matrix (ECM) genes that make up muscle connective
46 tissue (Vallecillo-Garcia, et al., 2017). In young adults, FAPs are necessary for normal growth
47 and long-term maintenance of skeletal muscle, which otherwise undergo progressive muscle
48 atrophy in the absence of PDGFRα$^{+}$ FAPs (Roberts, et al., 2013; Wosczyna, et al., 2019;
49 Uezumi, et al., 2021). Upon muscle injury, FAPs proliferate in response to IL-4/IL-13 signals
50 from eosinophils, and participate in clearing of necrotic debris via phagocytosis (Heredia, et
51 al., 2013). Also, the proliferated FAPs regulate expansion and asymmetric commitment of
52 muscle stem cells (MuSCs) via secreted factors such as WISP1, leading to robust *de novo*
53 myofiber formation (Joe, et al., 2010; Lukjanenko, et al., 2019; Wosczyna, et al., 2019).
54 Conversely, absence of FAPs or its functional decline with age cause premature differentiation
55 of MuSCs upon injury, resulting in formation of smaller regenerated myofibers (Murphy, et al.,
56 2011; Lukjanenko, et al., 2019; Wosczyna, et al., 2019). After sufficient regeneration of
57 myofibers occurs, FAPs undergo apoptosis via TNF signaling from monocyte/macrophages,
58 such that its numbers return to those of unperturbed muscles (Lemos, et al., 2015; Saito, et al.,
59 2020). Failure to remove excess FAPs after muscle regeneration results in unwanted fibrosis,
60 which compromises muscle function (Uezumi, et al., 2011; Uezumi, et al., 2014).

61

62 In addition to formation and maintenance of muscle tissue, FAPs also contribute to maturation
63 and maintenance of the neural components within skeletal muscle. Previously, we reported that
64 FAPs promote postsynaptic maturation of the neuromuscular junction (NMJ) through the
65 BAP1/SMN axis during postnatal development (Kim, et al., 2022). Selective inactivation of
66 *Bap1* in FAPs results in dysfunctional NMJs, with sustained expression of the immature form
67 of acetylcholine receptor subunit, *AchRγ*, in skeletal muscle (Kim, et al., 2022). Progressively,
68 these mice exhibit denervation at the NMJ, retraction of motor axons, reduction of myelination
69 and axon diameter, and eventually motor neuron loss, suggesting that FAPs prevent the dying-
70 back loss of motor neurons (Kim, et al., 2022). Recently, we also reported defective presynaptic
71 maturation and maintenance in mice with selective *Smn* downregulation in FAPs, again
72 suggesting the role of FAPs in postnatal NMJ development (Hann, et al., 2023). In adult mice,
73 BMP3B secretion by FAPs stabilize NMJs and Schwann cells by promoting the myelination
74 program in Schwann cells, thereby directly contributing to the maintenance of neural
75 components within skeletal muscle (Uezumi, et al., 2021). In the absence of FAPs or *Bmp3b*,
76 mice exhibit muscle weakness and myofiber atrophy along with destabilization of Schwann
77 cells and denervation at NMJs, which closely resemble the phenotypes observed in age-related
78 sarcopenia (Uezumi, et al., 2021). Similarly, conditional deletion of *Bap1* in FAPs in adulthood
79 cause denervation at the NMJs and eventually loss of motor neurons, demonstrating the
80 requirement of FAPs in maintaining the neuromuscular system (Kim, et al., 2022). Conversely,
81 disturbance in the neural component can influence the behavior of FAPs; for instance,
82 denervation is known to activate FAPs (Contreras, et al., 2016; Gonzalez, et al., 2017; Madaro,
83 et al., 2018). This suggests that FAPs can somehow sense the anatomically distant peripheral
84 nerve injury. However, the question of how FAPs are able to sense the distant peripheral nerve

injury remains unanswered (Theret, et al., 2021). Furthermore, whether FAPs are actually able to exert beneficial effects on peripheral nerve regeneration remains elusive.

In accordance with its various functions, heterogeneity within FAPs began to be recognized with the advent of single-cell analysis technology (Contreras, et al., 2021). By profiling the expression levels of 87-selected genes in isolated singlets of FAPs, dynamic transitions between heterogeneous subpopulations of FAPs, identified by different expression levels of TIE2 and VCAM1, was observed during postnatal and regenerative myogenesis (Malecova, et al., 2018). The report showed that while activation of TIE2$^{high}$ FAPs is observed in neonatal mice, activation of VCAM1$^{+}$ FAPs is observed in injured muscles, suggesting distinct functional involvement of FAPs in the two different contexts of myogenesis (Malecova, et al., 2018). Additionally, single-cell RNA-sequencing (scRNA-seq) enabled identification of heterogeneity within FAPs based on the genome-wide transcriptome data (Lieberman, et al., 2021). In homeostatic adult muscle, two distinct subpopulations within FAPs have been identified, namely *Dpp4*$^{+}$ and *Cxcl14*$^{+}$ FAPs (Scott, et al., 2019; Oprescu, et al., 2020). Functionally, we reported that DPP4$^{+}$ FAPs contribute to maturation and maintenance of the neuromuscular system via the BAP1/SMN axis (Kim, et al., 2022). In juvenile muscle, five different subpopulations within FAPs were characterized, each having different contexts of activation and differentiation potentials (Leinroth, et al., 2022). *Osr1*$^{+}$ FAPs are precursor cells that can form all other subpopulations; *Clu*$^{+}$ FAPs are most potent in mineralization; *Adam12*$^{+}$ and *Gap43*$^{+}$ FAPs are immune-responsive; and *Hsd11b1*$^{+}$ FAPs respond to nerve transection (Leinroth, et al., 2022). The different activation cues and differentiation potentials in each subpopulation of FAPs suggest distinct roles those subsets can play in different contexts of

skeletal muscle biology. Indeed, dynamic transcriptomic changes in FAP subpopulations in response to muscle injury (Scott, et al., 2019; De Micheli, et al., 2020; Oprescu, et al., 2020) or denervation (Nicoletti, et al., 2020; Proietti, et al., 2021; Lin, et al., 2022; Nicoletti, et al., 2023) have been identified in studies that implemented scRNA-seq analysis. Still, the question of how FAPs may sense the distant nerve injury and whether FAPs can beneficially contribute to nerve regeneration remain largely unknown.

Here, using the scRNA-seq approach, we aimed to identify the response mechanism of FAPs to nerve injury, by uncovering its nerve injury-sensing mechanism and its potentially beneficial effect on nerve regeneration. To obtain a comprehensive scRNA-seq database of FAPs' response to nerve injury, FAPs from both chronic, non-regenerating nerve injury (denervation)- and acute, regeneration-prone nerve injury (crush)-affected muscles were collected at different time points over the course of regeneration. As a result, distinct transcriptomic profiles of FAPs at different time points post the two types of nerve injuries were captured in single-cell resolution, from which the response mechanism of FAPs to nerve injury was identified and validated using mouse models. Specifically, we found that upon peripheral nerve injury, GDNF from Schwann cells can activate FAPs, which in turn express BDNF to promote remyelination during nerve regeneration. Our study suggests FAPs as an important player that actively participates in the nerve regeneration process, of which we believe should be considered in future studies aiming for improved understanding of the peripheral nerve regeneration process.

## Results

### Distinct response profiles of FAPs upon nerve crush injury versus denervation

To establish a comprehensive transcriptome database of nerve injury-affected FAPs at single-cell resolution, we performed scRNA-seq using FAPs isolated from sciatic nerve crush injury (SNC)- or denervation (DEN)-affected muscles at different time points over the course of regeneration (Figure 1—figure supplement 1A and B). Four time points (3, 7, 14, and 28 days post injury, hereafter dpi) along the regeneration process were chosen for analysis to capture the transcriptomes of FAPs at both early and late stages of regeneration. Selection of such time points was based on a previous report that showed the reinnervation process of the tibialis anterior (TA) muscle after SNC, where Wallerian degeneration was evident at 7 dpi, and reinnervation was mostly completed at 28 dpi (Magill, et al., 2007). Including the uninjured control, scRNA-seq data from a total of nine samples (Uninjured, SNC-3dpi, SNC-7dpi, SNC-14dpi, SNC-28dpi, DEN-3dpi, DEN-7dpi, DEN-14dpi, and DEN-28dpi) were obtained via the 10x Genomics platform (Figure 1—figure supplement 1A). Quality control and filtering of the sequenced cells yielded a total of 44,597 cells for further analysis, where 4955.2±1022.8 cells were captured from each sample. Prior to downstream analysis, integration (Hao, et al., 2021) of our scRNA-seq data with a publicly available scRNA-seq data of mononuclear cells from denervated muscles at 0, 2, 5, and 15 dpi (Nicoletti, et al., 2023) was carried out for data validation. Expectedly, most (97.7%) of the filtered cells in our scRNA-seq data clustered with the denervation-affected FAPs in the published scRNA-seq data, confirming the validity of the data produced in our study (Figure 1—figure supplement 1C and D).

152 To look into the chronological transcriptomic changes that occur in FAPs in response to SNC
153 or DEN on a global level, we analyzed our scRNA-seq data by samples. Visualization of the
154 scRNA-seq data on uniform manifold approximation and projection (UMAP) plots showed
155 similar changes in the early stages of regeneration (3 and 7 dpi) compared to uninjured FAPs,
156 regardless of the type of injury (Figure 1A). However, as FAPs reached later stages of
157 regeneration (14 and 28 dpi), SNC-affected FAPs returned to states similar to uninjured control,
158 while DEN-affected FAPs stayed in the activated state (Figure 1A). The similarities and
159 differences observed on the UMAP plots could also be found in the differentially expressed
160 gene (DEG) analyses as well as in the hierarchical clustering analysis using those DEGs (Figure
161 1B–E, Figure 1—figure supplement 2A–C). As a result of pairwise DEG analyses comparing
162 all nine samples, different numbers of DEGs were identified, of which correlated with the
163 similarities between samples observed on UMAP plots (Figure 1A–E, Figure 1—figure
164 supplement 2A and B). Hierarchical clustering of the nine samples using all unique DEGs
165 identified from the pairwise comparisons showed clustering of uninjured control with SNC-
166 14dpi and SNC-28dpi, suggesting FAPs' return to homeostatic state (Figure 1—figure
167 supplement 2C). On the other hand, DEN-14dpi and DEN-28dpi clustered with each other, but
168 not with uninjured control, suggesting the chronic activation of FAPs in response to DEN as
169 reported previously (Madaro, et al., 2018) (Figure 1—figure supplement 2C). Samples that
170 captured the early responses of FAPs to nerve injuries (3 or 7 dpi) were clustered together by
171 dpi rather than the type of injury, suggesting similar response profiles of FAPs to both types of
172 nerve injuries (Figure 1—figure supplement 2C). Indeed, the numbers of DEGs between SNC-
173 3dpi versus DEN-3dpi and SNC-7dpi versus DEN-7dpi were among the lowest identified in
174 the pairwise analyses (Figure 1B and C, Figure 1—figure supplement 2A). Overall, the number
175 of DEGs between SNC- and DEN-affected FAPs increased significantly with dpi, showing the

176 bifurcation of FAP's response to the different types of nerve injuries in the later stages of
177 regeneration (Figure 1B–E).

178

179 In a previous study, chronic activation of the STAT3/IL-6 pathway in FAPs in response to DEN
180 was reported (Madaro, et al., 2018). Indeed, *Il6* was identified as one of the genes upregulated
181 at all four time points in response to DEN compared to uninjured control in our data (Figure
182 1—figure supplement 2D and E). Although it did not pass the fold change (FC) threshold (FC
183 >= 2) in the DEG analyses, expression of *Stat3* also showed significant chronic upregulation
184 in all DEN-affected FAPs as well (Figure 1—figure supplement 2F and G). In response to SNC,
185 however, only transient upregulation of both genes was observed (Figure 1—figure supplement
186 2D–G).

187

188 To obtain biological insights on the different responses of FAPs to SNC versus DEN in the later
189 stage of regeneration, we subjected the two lists of genes from Figure 1E (28 dpi, SNC_UP and
190 DEN_UP) to gene set overrepresentation analysis (ORA) using g:Profiler (Kolberg, et al.,
191 2023). From both sets of genes, pathways related to tissue regeneration/wound healing were
192 enriched (Figure 1F and G, Figure 1—figure supplement 3A and B). In contrast, pathways
193 related to immune cell recruitment, inflammation, and ECM regulation by collagen
194 biosynthesis were enriched specifically in DEN-28dpi (Figure 1F, Figure 1—figure supplement
195 3A), which is consistent with the previous report that showed the direct contribution of FAPs
196 to fibrosis in denervated muscles (Contreras, et al., 2016; Madaro, et al., 2018). Also, mild
197 immune cell infiltration into affected muscles in response to DEN was previously described
198 (Lin, et al., 2022; Nicoletti, et al., 2023); our results suggest the role of FAPs in chemotactic

199 recruitment of immune cells in denervated muscles. In addition, the pathway 'negative
200 regulation of neuron apoptosis' was enriched in DEN-28dpi, suggesting a prolonged attempt
201 of FAPs to preserve neurons that must be alive for reinnervation of the denervated muscle
202 (Figure 1F, Figure 1—figure supplement 3A). On the other hand, some pathways were
203 exclusively enriched in SNC-28dpi, such as negative regulation of chemotaxis and
204 prostaglandin metabolism (Figure 1G, Figure 1—figure supplement 3B). It is generally
205 understood that after a successful tissue regeneration process, resolution of immune response
206 allow for the tissue to return to homeostasis (Ortega-Gomez, et al., 2013; Aurora and Olson,
207 2014; Julier, et al., 2017); our results suggest the role of FAPs in regulating immune resolution
208 near the end of nerve regeneration. Furthermore, the role of prostaglandin in peripheral nerve
209 regeneration has recently been described (Forese, et al., 2020; Bakooshli, et al., 2023); our
210 ORA results suggested that FAPs may also be involved in regulation of prostaglandin levels
211 during peripheral nerve regeneration.

212

213 To discover biological pathways behind the supposedly similar responses of FAPs to both SNC
214 and DEN in the early phases of regeneration, we examined DEGs from comparing SNC-3dpi,
215 SNC-7dpi, DEN-3dpi, and DEN-7dpi to uninjured controls. Many of the upregulated genes
216 identified in the DEG analyses were shared amongst the four samples (Figure 1—figure
217 supplement 3C). ORA using the shared upregulated genes revealed enrichment in pathways
218 that were also enriched in DEN-28dpi compared to SNC-28dpi, such as immune cell
219 recruitment and ECM regulation, supporting the idea that early-activated states within FAPs
220 persist for a prolonged period in response to DEN (Figure 1F and H, Figure 1—figure
221 supplement 3A and D). Collectively, analysis of our scRNA-seq data by samples revealed

222 similar response profiles of FAPs to both SNC and DEN in the early stages of regeneration,
223 which then bifurcated into chronic activation in response to DEN and return to homeostasis in
224 response to SNC, showing correlative behaviors along with the degree of nerve regeneration
225 and target muscle reinnervation.

226

227 **Nerve injury-responsive subsets within FAPs**

228 Although analysis of our scRNA-seq data on the population level provided general insights on
229 how FAPs may respond to the different types of nerve injuries, the results could not provide us
230 with sufficient clues on how FAPs can sense nerve injuries, or how they may directly contribute
231 to nerve regeneration. Thus, we next analyzed our scRNA-seq data on the subpopulation level,
232 hoping to distinguish subsets within FAPs that may be more relevant to the context of sensing
233 and responding to nerve injury. To identify distinct subsets within nerve injury-affected FAPs,
234 we applied unsupervised clustering to the merged scRNA-seq data of all nine samples
235 following the Seurat-R workflow (Hao, et al., 2021). As a result, seven clusters with unique
236 gene expression profiles were identified from the nerve injury-affected FAPs, with marker
237 genes specifically expressed in each cluster (Figure 2A–C, Figure 2—figure supplement 1A).

238

239 Interestingly, while clusters 4-7 showed little or no significant change in their proportions in
240 response to nerve injury, clusters 1-3 exhibited dramatic changes upon nerve injury (Figure 2D
241 and E). In particular, cluster 1 was mostly present in uninjured muscles or in muscles where
242 reinnervation had occurred to at least some degree (SNC-14dpi and SNC-28dpi) (Magill, et al.,
243 2007) (Figure 2D and E). In contrast, presence of clusters 2 and 3 were mutually exclusive to

244 cluster 1, such that their appearances were transient in response to SNC and chronic upon DEN
245 (Figure 2D and E). Based on this mutual exclusivity of the three clusters, we speculated that
246 cluster 1 can sense and respond to nerve injuries, and that clusters 2 and 3 may have arisen
247 from cluster 1 upon nerve injury.

248

249 To obtain clues on whether such changes between FAP clusters could have actually occurred
250 in response to nerve injury, we first performed RNA velocity analysis using R package
251 velocyto.R (La Manno, et al., 2018). RNA velocities on the UMAP plots predicted
252 transcriptomic flow from cluster 1 to clusters 2 and 3 in the early stages of regeneration in both
253 SNC- and DEN-affected FAPs, which was in line with our speculation (Figure 2—figure
254 supplement 1B). Conversely, transcriptomic flow from clusters 2 and 3 back to cluster 1 was
255 evident in SNC-affected FAPs in the later stages of regeneration (Figure 2—figure supplement
256 1B). However, RNA velocities in DEN-affected FAPs were represented as dots instead of
257 arrows on clusters 2 and 3 in the later stages, suggesting an unchanging, chronic state of their
258 transcriptomes, which is consistent with the chronic activation of FAPs in response to DEN
259 (Madaro, et al., 2018) (Figure 2—figure supplement 1B). Additionally, hierarchical clustering
260 of the seven FAP clusters using DEGs enriched in each cluster grouped clusters 1-3 together,
261 supporting our speculation that clusters 2 and 3 originate from cluster 1 (Figure 2—figure
262 supplement 1C). Recently, *Hsd11b1*-expressing FAPs were identified as the FAP subset that is
263 specifically activated in response to nerve transection injury (Leinroth, et al., 2022). Since we
264 speculated that cluster 1 in our scRNA-seq data can sense and respond to nerve injury, we
265 examined the expressions of marker genes identified in the previous report – *Hsd11b1*, *Mme*,
266 *Ret*, and *Gfra1* (Leinroth, et al., 2022) – in our scRNA-seq data. Indeed, all four markers were

enriched in cluster 1 in our data (Figures 3A and B, Figure 2—figure supplement 1D–F). Expressions of marker genes *Hsd11b1* and *Mme* were also enriched in clusters 2 and 3, further supporting the idea that those clusters may have arisen from cluster 1 (Figure 2—figure supplement 1D–F). Together, these data suggest that clusters 1-3 are the dynamic interchanging subsets of FAPs that specifically respond to nerve injury, where cluster 1 senses nerve injuries in unperturbed muscles and clusters 2 and 3 arise from cluster 1 to respond to nerve injury.

**GDNF signaling pathway in the nerve injury-sensing mechanism by FAPs**

Among the four marker genes expressed in cluster 1, *Ret* and *Gfra1* are well-known as GDNF receptors, where Gfra1 directly binds GDNF, which in turn activates the receptor tyrosine kinase (RTK) Ret for downstream signal transduction (Jing, et al., 1996; Treanor, et al., 1996; Trupp, et al., 1996). Meanwhile, robust but specific expression of GDNF by Schwann cells in response to peripheral nerve injury has been reported (Hammarberg, et al., 1996; Hoke, et al., 2002; Arthur-Farraj, et al., 2012; Xu, et al., 2013; Proietti, et al., 2021). Accordingly, we presumed that FAPs, especially the *Ret*- and *Gfra1*-expressing cluster 1 cells, may sense the distant nerve injury by detecting GDNF secreted from Schwann cells. Notably, both *Ret* and *Gfra1* were among the top 10 DEGs specifically enriched in cluster 1, suggesting that they can readily respond to GDNF (Figure 2C, Figure 3—figure supplement 1A). In addition, comparing the expression levels of *Ret* and *Gfra1* in skeletal muscle-resident mononuclear cell populations isolated by fluorescence-activated cell sorting (FACS) revealed robust co-expression of both genes in FAPs, but not as much in other cell populations (Figure 3C and D). Thus, FAPs may be the main cell type within skeletal muscle that can respond to GDNF secreted by Schwann cells in case of a nerve injury.

290

291 To further investigate the relevance of GDNF signaling in the nerve injury-sensing mechanism
292 by FAPs, we subjected lists of DEGs enriched in clusters 1-3 to ORA. Genes enriched in cluster
293 1 returned pathways 'GDNF receptor signaling pathway', 'regulation of cellular response to
294 growth factor stimulus', and 'positive regulation of peptidyl-tyrosine phosphorylation', where
295 tyrosine residues on the RTK Ret is known to be phosphorylated upon activation (Jing, et al.,
296 1996; Treanor, et al., 1996; Trupp, et al., 1996) (Figure 3—figure supplement 1B). The two
297 latter pathways were also found in the ORA results using DEGs enriched in clusters 2 and 3,
298 supporting the idea that those clusters originate from cluster 1 upon nerve injury (Figure 3E,
299 Figure 3—figure supplement 2A and B). The pathway 'positive regulation of ERK1/2 cascade'
300 was enriched in cluster 2, suggesting the involvement of GDNF-Ret-Ras-ERK signaling
301 cascade within the MAPK signaling pathway in this cluster (Airaksinen and Saarma, 2002;
302 Sariola and Saarma, 2003; Kanehisa, et al., 2023) (Figure 3G, Figure 3—figure supplement 1C
303 and 2A). In addition to ORA, we predicted upstream transcription factors (TFs) that could have
304 regulated the expressions of the DEGs enriched in the two activated FAP subsets, clusters 2
305 and 3, using TRRUST (Han, et al., 2018). As a result, TFs *Fos*, *Jun* and *NF-κB* (*Nfkb1, Nfkb2*)
306 were predicted from both lists of DEGs, all of which are known to act downstream of the
307 GDNF/Ret-induced MAPK signaling pathway (Fielder, et al., 2018; Kanehisa, et al., 2023)
308 (Figure 3F and G, Figure 3—figure supplement 1C, Supplemental tables 1 and 2). Collectively,
309 robust and specific co-expression of GDNF receptors in cluster 1, together with the prediction
310 of RTK activation and involvement of GDNF signaling pathway downstream TFs in clusters 2
311 and 3, suggests that GDNF signaling could be the mechanism by which FAPs sense the distant
312 nerve injury, where local Schwann cells act as the GDNF source upon nerve injury.

313

314 ***Bdnf* expression in FAPs by both endogenous and exogenous GDNF**

315 Next, to discover how FAPs may contribute to nerve regeneration, we screened the list of genes
316 enriched in clusters 2 and 3 that were predicted to be downstream of the GDNF signaling
317 pathway to identify candidate effector genes. From the TRRUST analysis results, 44 genes
318 were identified to be regulated by either *Fos*, *Jun*, or *NF-κB* (Figure 4A, Supplemental tables
319 1–3). Since FAPs themselves do not constitute the neural components within skeletal muscle,
320 we reasoned that secreted factors from FAPs would most likely exert beneficial effect on the
321 regenerating nerves. Also, considering the effector gene's potential function in supporting
322 nerve regeneration, we presumed that it regulates neurons or glial cells. Moreover, we
323 anticipated that expression of the effector gene would be limited to the context of nerve injury
324 and regeneration, since the vast majority of FAPs are in a quiescent state in unperturbed adult
325 musclesScott, et al., 2019. Thus, we applied the following criteria to narrow down our
326 candidate gene list: (1) genes that are known to code secreted proteins, (2) genes that are known
327 to regulate neurons or glial cells, and (3) genes that are expressed exclusively in activated FAPs
328 in response to nerve injury (Figure 4A, Supplemental table 3). Unexpectedly, after filtering out
329 genes that did not fit the three criteria, only *Bdnf* remained in our candidate gene list that could
330 act as the effector secreted by FAPs upon nerve injury to support nerve regeneration (Figure
331 4A). Expression patterns of *Bdnf* in FAPs upon nerve injury showed transient upregulation in
332 SNC-affected FAPs, whereas chronic expression of *Bdnf* was observed in DEN-affected FAPs,
333 showing correlation with its potential requirement during nerve regeneration (Figure 4C). The
334 expression of *Bdnf* was mostly limited to cluster 2 (Figure 4B), where pathway analysis and
335 TF prediction suggested the involvement of GDNF-Ret-Ras-ERK-Fos signaling cascade in this

336 subset of FAPs (Figure 3F and G, Figure 3—figure supplement 1C and 2A). Accordingly, we
337 hypothesized that FAPs secrete BDNF in response to GDNF from Schwann cells upon nerve
338 injury, to actively take part in the regeneration process.

339

340 To validate our hypothesis *in vivo*, we first examined the expression profiles of *Gdnf* in
341 Schwann cells and *Bdnf* in FAPs at early time points in response to SNC, using $Plp1^{CreER}$;
342 $Rosa^{tdTomato}$ mice to specifically label and hence isolate Schwann cells (Doerflinger, et al., 2003)
343 (Figure 4D). Expectedly, we could observe sequential upregulation of *Gdnf* and *Bdnf* from
344 Schwann cells and FAPs, respectively, where *Gdnf* levels peaked at 1 dpi in Schwann cells,
345 followed by a gradual increase of *Bdnf* expression in FAPs, which peaked at 3 dpi (Figures 4D
346 and E). In addition, to validate the sufficiency of GDNF signaling in inducing *Bdnf* expression
347 in FAPs *in vivo*, we injected recombinant mouse GDNF protein into the TA and the two
348 gastrocnemius (GA) muscles (lateral and medial GA), from which FAPs were FACS-isolated
349 48 hours post injection to investigate the expression of *Bdnf* (Figure 4F). Compared to PBS
350 control, intramuscular injection of GDNF sufficiently induced *Bdnf* expression in FAPs, even
351 in the absence of a nerve injury (Figure 4F and G). Together, we suggest that FAPs can respond
352 to nerve injury via the GDNF-BDNF axis, since recombinant GDNF protein could sufficiently
353 induce *Bdnf* expression in FAPs without nerve injury, and sequential upregulation of *Gdnf* and
354 *Bdnf* could be observed from Schwann cells and FAPs following nerve injury, respectively.

355

356 **Remyelination by FAP-derived BDNF during peripheral nerve regeneration**

357 Although BDNF is known to function in processes such as axon elongation (Oudega and Hagg,
358 1999; English, et al., 2013), survival of neurons (Ghosh, et al., 1994; Baydyuk and Xu, 2014),
359 and myelination by Schwann cells (Zhang, et al., 2000; Xiao, et al., 2009), the role of BDNF
360 secreted by FAPs in nerve regeneration is unknown. To find out how FAP-derived BDNF can
361 contribute to nerve regeneration, we produced conditional knockout (cKO) mice where *Bdnf* is
362 specifically inactivated in mesenchymal progenitors including FAPs, by crossing *Prrx1*$^{Cre}$ mice
363 (Logan, et al., 2002; Kim, et al., 2022; Leinroth, et al., 2022; Hann, et al., 2023) with *Bdnf*-
364 floxed (*Bdnf*$^{fl}$) mice (*Prrx1*$^{Cre}$; *Bdnf*$^{fl/fl}$, hereafter cKO) (Figure 5—figure supplement 1A).
365 Inactivation of *Bdnf* in FAPs in the cKO mice was confirmed on both genomic DNA and mRNA
366 levels (Figure 5—figure supplement 1B and C). Though Cre expression in *Prrx1*-expressing
367 cells occur from embryonic day 9.5 (Logan, et al., 2002), no visible phenotypes were observed
368 in the postnatal, juvenile and adult cKO mice compared to littermate controls (hereafter, Ctrl).
369 However, upon SNC in the right hindlimb, cKO mice displayed a delay in nerve regeneration
370 compared to Ctrl, measured by compound muscle action potential (CMAP) amplitude and
371 latency via electromyography (EMG) on the GA muscle (Figure 5A–5D, Figure 5—figure
372 supplement 1D and E). At 4 weeks post injury (wpi), nerve regeneration in both Ctrl and cKO
373 mice showed insufficient recovery in the right, injured GA compared to the left, uninjured GA,
374 where lower amplitude and prolonged latency in CMAP was observed (Figure 5B–D).
375 However, at 6 wpi, while CMAP amplitude and latency in the left and right GAs became
376 comparable in Ctrl mice, recovery of such values were stalled at levels comparable to 4 wpi in
377 the cKO mice (Figure 5B–D). By 12 wpi, electrophysiological functions of the injured nerves
378 became statistically comparable to that of its contralateral counterpart in the cKO mice,
379 indicating a delayed regeneration in the cKO mice (Figure 5B–D).

380

381 Generally, decrease in CMAP amplitude and prolonged CMAP latency can be explained by
382 two main causes: axonal loss and defective myelination (Mallik and Weir, 2005; Chung, et al.,
383 2014). Since complete regeneration of the injured nerves on the electrophysiological level
384 could be achieved after a sufficient period of time in the cKO mice (Figure 5B–D), we
385 presumed that axonal loss would not have occurred, since it would result in permanent defects
386 by loss of motor units. Instead, we thought that defective myelination could have occurred in
387 the cKO mice, considering the fact that BDNF is already known to promote remyelination
388 during peripheral nerve regeneration (Zhang, et al., 2000; Zheng, et al., 2016), and that
389 defective myelination alone can affect both CMAP amplitude and latency (Mallik and Weir,
390 2005). Thus, we investigated the effect of conditional *Bdnf* inactivation in FAPs on regenerative
391 myelination by examining the sciatic nerves from Ctrl versus cKO mice at 6 wpi, when the
392 delayed functional recovery of the injured nerves in the cKO mice was prominent (Figure 5A–
393 D). Toluidine blue staining of the semi-thin sections of injured sciatic nerves revealed
394 significantly reduced myelin thickness in the cKO mice compared to Ctrl mice (Figure 5E).
395 Indeed, higher G-ratio values were calculated from cKO mice compared to Ctrl, confirming
396 the reduced myelination in the regenerating nerves in cKO mice (Figure 5F, Figure 5—figure
397 supplement 1F and G). This decrease in myelin thickness was independent from axon diameter,
398 which were comparable in both Ctrl and cKO mice, implying that no axonal loss or defect had
399 occurred in the cKO mice compared to controls (Figure 5G). Taken together, our results
400 revealed the direct involvement of FAP-derived BDNF in the remyelination process during
401 peripheral nerve regeneration, such that inadequate levels of *Bdnf* expression in FAPs caused
402 delayed remyelination and hence delayed nerve regeneration in the cKO mice.

403

404 **Implication of FAP-derived BDNF in the age-related delay in nerve regeneration**

405 Finally, to seek clinical relevance of *Bdnf* expression in FAPs during nerve regeneration, we
406 compared the expression levels of *Bdnf* in adult (5-6 months) versus aged (24 months) mice in
407 FAPs post SNC. At 7 dpi, *Bdnf* expression was significantly reduced in the aged mice compared
408 to adult mice (Figure 6A and B). Such a difference could be one of the factors that lead to the
409 delayed or failed regeneration of injured nerves in the elderly compared to healthy, young
410 adults, suggesting the clinical role of FAPs in a timely, successful peripheral nerve regeneration
411 process.

412

413 **Discussion**

414 Traumatic injury to the peripheral nerve has severe consequences, including lifelong paralysis
415 of the injured limb that can compromise the quality of life significantly (Grinsell and Keating,
416 2014). Thus, understanding the regeneration process of the peripheral nerves is fundamental
417 for treating the potentially devastating injury. Previously, several cellular components in and
418 outside the injured nerve were discovered to actively participate in the regeneration process,
419 including the injured neurons (Hanz, et al., 2003), glial cells (Arthur-Farraj, et al., 2012),
420 immune cells (Mueller, et al., 2001; Kalinski, et al., 2020), and nerve-resident mesenchymal
421 cells (Parrinello, et al., 2010; Toma, et al., 2020), via diverse mechanisms so that the nerve can
422 regain its function (Scheib and Hoke, 2013). In this study, we investigated the response
423 mechanism of muscle-resident FAPs to both acute and chronic peripheral nerve injury via
424 scRNA-seq, and revealed that this population of cells can also actively take part in the nerve

425 regeneration process. Here, we discovered that muscle-resident FAPs can recognize the distant
426 nerve injury by sensing GDNF secreted by Schwann cells. Though GDNF secretion by
427 Schwann cells in response to nerve injury had previously been recognized (Hammarberg, et al.,
428 1996; Hoke, et al., 2002; Arthur-Farraj, et al., 2012; Xu, et al., 2013; Proietti, et al., 2021), we
429 identified FAPs as a major target cell population of GDNF within skeletal muscle, based on the
430 enriched expression of GDNF receptors. In depth, exploiting the technical advantage of
431 scRNA-seq, we suggested that a subset of FAPs, named cluster 1 in this study, can sense the
432 local GDNF by expressing GDNF receptors *Ret* and *Gfra1*, and that upon GDNF sensing,
433 cluster 1 FAPs turn into clusters 2 and 3 to contribute to the nerve regeneration process.
434 Specifically, we discovered that FAPs, especially the *F2rl1*-expressing cluster 2, express *Bdnf*
435 in response to nerve injury and/or GDNF, which in turn was shown to promote the
436 remyelination process by Schwann cells during nerve regeneration, using our cKO mouse
437 model (Figure 6C). Since epineurial and perineurial, but not endoneurial mesenchymal cells
438 share their origins with the muscle-resident FAPs and therefore are *Prrx1*-positive (Joseph, et
439 al., 2004; Carr, et al., 2019), the possibility that the delayed remyelination observed in our cKO
440 mice could be due to the combined effect of *Bdnf* depletion in both muscle- and nerve-resident
441 mesenchymal cells cannot be eliminated. To resolve such issue, further investigations using
442 muscle-resident FAP-specific Cre mouse lines is required, but such line is currently unavailable
443 as no such specific marker has been found. Nevertheless, our findings show that muscle-
444 resident FAP-derived BDNF is indeed important for nerve regeneration, since intramuscular
445 injection of recombinant BDNF can sufficiently accelerate the nerve regeneration process
446 (Zheng, et al., 2016). Conversely, intramuscular injection of BDNF-neutralizing antibodies can
447 sufficiently delay nerve regeneration (Zheng, et al., 2016). Thus, endogenous supply of
448 intramuscular BDNF by the muscle-resident FAPs in our Ctrl mice would likely have supported

449 remyelination by Schwann cells, while the lack of such BDNF supply by FAPs in our cKO
450 mice would have resulted in delayed remyelination. Also, we found that while muscle-resident
451 FAPs robustly express both GDNF receptor genes, neither epineurial nor perineurial
452 mesenchymal cells express significant levels of *Ret* and *Gfra1* (Supplemental figure 1),
453 implying that the GDNF-BDNF axis found in this study could be valid uniquely in muscle-
454 resident FAPs. Collectively, we suggest that muscle-resident mesenchymal progenitors can
455 directly contribute to nerve regeneration via the GDNF-BDNF axis (Figure 6C), of which was
456 previously unidentified; we suggest that in future studies regarding peripheral nerve
457 regeneration, active participation of this intramuscular mesenchymal population should be
458 taken into consideration. In that process, our scRNA-seq data may provide valuable insights,
459 which may lead to additional discoveries on FAP's contributions to nerve regeneration by other
460 mechanisms, and/or provide clues on the cell-to-cell communications of FAPs with other cell
461 types that may lead to facilitation of the regeneration process.

462

463 Here, we have primarily investigated the roles of *Ret*-expressing and *F2rl1*-expressing FAPs
464 in sensing and responding to nerve injury, respectively. However, possibilities that other
465 subpopulations can exert distinct beneficial effects on nerve regeneration remain largely
466 unexplored. For example, although identified as a nerve injury-relevant subpopulation in this
467 study, specific contributions of the *Alkal2*-expressing cluster 3 FAPs to nerve regeneration are
468 yet to be discovered. Identification of effector genes such as *Bdnf* from this subpopulation may
469 lead to the discovery of an additional mechanism by which FAPs can contribute to nerve
470 regeneration. Although other subpopulations (clusters 4-7) did not exhibit dramatic fluctuations
471 in population percentage, some of the genes expressed specifically in those subpopulations

472 showed patterns that followed the regeneration process (Supplemental figure 2). Such gene
473 expression patterns suggest subpopulation-specific functions even in the less dynamic
474 subpopulations within FAPs in peripheral nerve regeneration, and require further investigations
475 to reveal their possible contributions.

476

477 The role of BDNF in peripheral nerve regeneration has been identified previously, where it was
478 found to promote both intrinsic axonal regeneration in neurons as well as remyelination by
479 Schwann cells (Zhang, et al., 2000; Zheng, et al., 2016). In such circumstances, various cellular
480 sources of BDNF have been identified. Bone marrow transplantation of wild-type cells into
481 *Bdnf* heterozygotic knockout mice revealed the involvement of bone marrow-derived cells in
482 expressing *Bdnf* that can promote nerve regeneration in the sciatic nerve (Takemura, et al.,
483 2012). Schwann cells themselves are cellular sources of BDNF during nerve regeneration
484 (Wilhelm, et al., 2012). In this study, we showed that BDNF from FAPs can also promote
485 myelination of the regenerating axons post injury, suggesting FAPs as an additional cellular
486 source of BDNF in peripheral nerve regeneration. The existence of cellular sources of BDNF
487 other than FAPs such as Schwann cells would provide an explanation for the delayed, but not
488 failed, remyelination in our *Bdnf* cKO mice, where complete regeneration had occurred after a
489 sufficient amount of time, despite the lack of *Bdnf* expression in FAPs. Still, ablation of *Bdnf*
490 in FAPs displayed significant delays in the remyelination process during nerve regeneration,
491 suggesting their requirement in the timely regeneration process of injured nerves. Meanwhile,
492 scRNA-seq data of all mononuclear cells from denervated muscles (Nicoletti, et al., 2023)
493 suggested expression of *Bdnf* in tenocytes and pericytes in addition to Schwann cells and FAPs
494 (Supplemental figure 3A and B). Although this may imply the involvement of those cellular

495 components in providing BDNF for nerve regeneration, expression of *Bdnf* in such cells were
496 not altered as significantly in response to nerve injury as in FAPs or Schwann cells
497 (Supplemental figure 3C). Moreover, while *Ret*-expressing FAPs and Schwann cells are known
498 to be in proximity to the NMJ or relevant nerve regeneration sites (Leinroth, et al., 2022), such
499 locational enrichment of tenocytes and pericytes have not been reported so far. Thus, it is likely
500 that FAPs, together with Schwann cells, are the main sources of BDNF within skeletal muscle
501 that can act in the remyelination process during peripheral nerve regeneration.

502

503 Aging is one of the well-known factors that can slow down the nerve regeneration process
504 (Verdú, et al., 2008; Maita, et al., 2023). Since multiple cell types are known to participate in
505 this process (Scheib and Hoke, 2013), determination of the cell types that can cause age-related
506 delays in nerve regeneration is important for the development of therapeutic approaches
507 targeting the relevant cell types. Of note, previous research emphasized the importance of niche
508 factors, rather than the intrinsic regenerative capacity of the injured neurons, in the age-related
509 decline in nerve regeneration (Painter, et al., 2014). Specifically, inability of Schwann cells to
510 adopt repair cell phenotypes has been pointed out as one of the age-related changes (Painter, et
511 al., 2014; Wagstaff, et al., 2021). In addition, age-related changes in immune cells, especially
512 macrophages, were suggested as causal factors that delay nerve regeneration (Buttner, et al.,
513 2018). In particular, chronic inflammatory phenotypes were shown to interfere with the
514 remyelination process by Schwann cells (Buttner, et al., 2018), and failed macrophage
515 infiltration in the early stages of regeneration resulted in defective Wallerian degeneration and
516 myelin debris clearing (Scheib and Hoke, 2016). In addition to the involvement of Schwann
517 cells and immune cells, we have identified muscle-resident FAPs as an additional cellular

518 component that can contribute to nerve regeneration, by promoting remyelination via BDNF
519 secretion. Surprisingly, expression of *Bdnf* by FAPs was significantly reduced in aged mice
520 compared to adult mice, suggesting the clinical relevance of FAP's involvement in the age-
521 related delay in peripheral nerve regeneration. We believe that further studies on age-related
522 changes in FAPs may provide valuable clues to understanding clinical observations from aged
523 individuals, which can lead to development of additional therapeutic strategies that include
524 FAPs as target cells in treating both young and aged nerve injury patients.

525

526 **Materials and Methods**

527

528 ***Animals***

529 C57BL/6J (RRID:IMSR_JAX:000664), *Prrx1*$^{Cre}$ (RRID:IMSR_JAX:005584), *Bdnf*$^{fl}$
530 (RRID:IMSR_JAX:004339), *Plp1*$^{CreER}$ (RRID:IMSR_JAX:005975) and *Rosa*$^{tdTomato}$
531 (RRID:IMSR_JAX:007914) mice were all obtained from The Jackson Laboratory. To generate
532 *Prrx*$^{Cre}$; *Bdnf*$^{fl/fl}$ mice, *Prrx*$^{Cre/+}$; *Bdnf*$^{fl/+}$ males and *Bdnf*$^{fl/fl}$ females were crossed to avoid
533 germline recombination in the female reproductive cells, and littermates were used as controls.
534 To generate *Plp1*$^{CreER}$; *Rosa*$^{tdTomato}$ mice, *Plp1*$^{CreER/+}$ mice were crossed with *Rosa*$^{tdTomato/+}$ mice,
535 and the line was kept by breeding *Plp1*$^{CreER/+}$; *Rosa*$^{tdTomato/tdTomato}$ males and females. Only mice
536 that had the *Plp1*$^{CreER}$ allele was used. Primers used for genotyping are listed in Supplemental
537 table 4. All mice were bred on the B6 background, except for the *Prrx*$^{Cre}$; *Bdnf*$^{fl/fl}$ mice and
538 littermates that were kept in the mixed B6, 129S4 and BALB/c background. All mice were
539 housed in a specific-pathogen-free (SPF) animal facility, with 12-h light/12-h dark cycle at
540 room temperature (RT, 22°C) and 40~60% humidity, and were fed with normal chow diet and

541 water ad libitum. Tamoxifen administration, sciatic nerve crush injury, denervation and
542 intramuscular GDNF injections were all given to 3 to 4-month-old adult mice. When
543 comparing aged mice versus adult mice, 24-month-old and 5 to 6-month-old mice were used,
544 respectively. In all cases except for *Plp1*$^{CreER}$; *Rosa*$^{tdTomato}$ mice, male mice were used for the
545 experiments. No sex-specific differences were observed in experiments using *Plp1*$^{CreER}$;
546 *Rosa*$^{tdTomato}$ mice. All experimental procedures were approved by the Institutional Animal Care
547 and Use Committtee at Seoul National University and were carried out according to the
548 guidelines provided.

549

550 ***Tamoxifen administration***

551 To label Schwann cells, 3-month-old *Plp1*$^{CreER}$; *Rosa*$^{tdTomato}$ mice were administered orally with
552 tamoxifen (20 mg/ml in corn oil, 160 mg/kg body weight; Sigma-Aldrich) 3 times every other
553 day.

554

555 ***Sciatic nerve injury***

556 Mice were deeply anesthesized via intraperitoneal injection of Avertin (32 mg/ml, ~800 mg/kg;
557 Sigma-Aldrich), and the incision site on the posterior side of the right hindlimb was shaved
558 and depilated using surgical clippers and hair removal cream. After cleansing the incision site
559 with 70% ethanol, incision was made on the skin with surgical scissors and the biceps femoris
560 muscle was punctured open with fine-tip forceps to expose the sciatic nerve. For sciatic nerve
561 crush injury, the exposed nerve was crushed with fine forceps for 30 seconds at the site just
562 proximal to where the tibial, peroneal and sural nerves branched out from the sciatic nerve. For

563 denervation, ~5 mm of the sciatic nerve proximal from the crush injury site was cut and
564 removed. The punctured biceps femoris muscle and skin were then sutured, and the incision
565 site was sterilized with povidion-iodine.

566

567 ***Intramuscular injection of GDNF***

568 Tibialis anterior muscle and the two gastrocnemius muscles (GA, lateral and medial) were each
569 injected with 10 μl of either PBS or recombinant mouse GDNF (10 μg/ml, Sigma-Aldrich)
570 using 31-gauge insulin syringes without damaging any innervating nerves. The injected
571 muscles were then dissected 48 hours post injection for isolation of FAPs and further analysis.

572

573 ***Isolation of FAPs, Schwann cells and others***

574 Isolation of muscle-resident FAPs, Schwann cells and others was performed according to a
575 previously reported protocol (Liu, et al., 2015) with minor modifications. Muscles indicated in
576 each experiment were dissected, finely chopped with surgical scissors and washed with 10%
577 horse serum (Gibco), DMEM (HyClone) for further dissociation. Enzymatic dissociation was
578 carried out in 10% horse serum, DMEM containing collagenase II (800 U/ml, Worthington
579 Biochemical) and dispase II (1.1 U/ml, Gibco) for 40 minutes at 37°C with mild agitation, and
580 mechanical dissociation was performed by tituration of the dissociated solution with a 20-
581 gauge needle ten times. After filtering the solution through a 40 μm strainer, dissociated
582 mononuclear single cells were stained with the following antibodies: APC anti-mouse CD31,
583 APC anti-mouse CD45, PE anti-mouse TER-119, Biotin anti-mouse CD106 (Vcam1)
584 (Biolegend) and FITC anti-mouse Ly-6A/E (Sca1) (BD Pharmingen); 7-aminoactinomycin D

585 (7-AAD, Sigma-Aldrich) was added to stain dead cells. Gating strategies used for the isolation
586 of each cell type were as follows: FAPs, 7-AAD$^-$Ter119$^-$CD31$^-$CD45$^-$Vcam1$^-$Sca1$^+$; MuSCs,
587 7-AAD$^-$Ter119$^-$CD31$^-$CD45$^-$Vcam1$^+$Sca1$^-$; lineage-positive cells, 7-AAD$^-$Ter119$^-$CD31$^+$ or 7-
588 AAD$^-$Ter119$^-$CD45$^+$; double-negative cells, 7-AAD$^-$Ter119$^-$CD31$^-$CD45$^-$Vcam1$^-$Sca1$^-$. For
589 Schwann cells, 7-AAD$^-$tdTomato$^+$ cells were sorted from tamoxifen-administered *Plp1*$^{CreER}$;
590 *Rosa*$^{tdTomato}$ mice.

591

592 ***scRNA-seq library construction and sequencing***

593 FAPs were isolated from sciatic nerve crush injury-affected or denervated muscles on days 3,
594 7, 14 and 28 post injury using wild type B6 mice, so that a total of nine samples, including
595 uninjured control, were collected for library generation. For each sample, isolated FAPs were
596 pooled from two mice. Chromium Next GEM Single Cell 3′ Kit v3.1 (10x Genomics) was used
597 according to the manufacturer's instructions for the nine collected FAP samples, and target cell
598 number for recovery was set to 5,000 in each sample. Sequencing of the libraries was carried
599 out using HiSeq X Ten (Illumina).

600

601 ***Computational analysis of scRNA-seq data***

602 Sequenced reads were aligned to the mouse reference genome mm10 using CellRanger v3.1.0
603 (10x Genomics), and aligned reads were transformed into gene-cell count matrices using
604 velocyto v0.17 (La Manno, et al., 2018) to obtain count matrices for both spliced and unspliced
605 mRNAs. Output loom files were then loaded with R package SeuratWrappers v0.3.1, and were
606 preprocessed and analyzed using R package Seurat v4.3.0 (Hao, et al., 2021) for downstream

analysis. The preprocessing steps for quality control included doublet filtering, live cell filtering and removal of non-FAPs as previously described (Kim, et al., 2022). All nine sample data were merged and normalized for dimensionality reduction, where top 8 principal components from the principal component analysis using 5,000 variable genes were selected for 2-dimensional UMAP embedding and visualization. Unsupervised clustering of cells was achieved through FindNeighbors and FindClusters functions in Seurat R package. To identify DEGs in the pairwise comparisons of scRNA-seq samples, the FindMarkers function in Seurat R package was used with the following parameters: fold change >= 2, pseudocount.use = 0.01, min.pct = 0.01, adjusted p value < 0.05. For identification of DEGs in each cluster, FindAllMarkers function was used with the parameters: fold change >= 1.5, pseudocount.use = 0.01, min.pct = 0.02, adjusted p value < 0.05. For hierarchical clustering, R package pheatmap v1.0.12 was used. For RNA velocity analysis, R package velocyto.R v0.6 was used following the instructions provided by the developer (La Manno, et al., 2018). For the prediction of upstream regulatory transcription factors using lists of DEGs enriched in the selected FAP clusters, the web-based tool TRRUST v2 (Han, et al., 2018) was used. For color mapping of the MAPK signaling pathway, online version of the KEGG Mapper – Color (Kanehisa, et al., 2023) was used.

***Gene set overrepresentation analysis***

To identify pathways enriched in the lists of DEGs, web-based version of g:Profiler (Kolberg, et al., 2023) was used with the following parameters: organism – Mus musculus; ordered query – YES; data sources – GO biological process without electronic GO annotations, Reactome, and WikiPathways; advanced options were set to default. Visualization of the results were done

630 as previously described (Reimand, et al., 2019), using the Cytoscape v3.10.1 (Shannon, et al.,
631 2003) application with tools EnrichmentMap v3.3.6 (Merico, et al., 2010) and AutoAnnotate
632 v1.4.1 (Kucera, et al., 2016).

633

634 ***RNA extraction and qRT-PCR***

635 Total RNA extraction and reverse transcription was carried out for isolated FAPs, Schwann
636 cells, MuSCs and others using TRIzol™ reagent (Invitrogen) and ReverTra Ace™ qPCR RT
637 Master Mix (Toyobo) reagents respectively, following the manufacturer's instructions. qPCR
638 was performed using ORA™ SEE qPCR Green ROX L Mix (HighQu) reagent, with gene-
639 specific primers listed in Supplemental table 4. Quantitative analysis of mRNA levels were
640 done using the $2^{-\Delta\Delta Ct}$ method with β-actin (*Actb*) as the housekeeping gene for normalization.

641

642 ***Electromyography and CMAP measurement***

643 Intraperitoneal injection of Avertin (32 mg/ml, ~800 mg/kg) for anesthetization of mice was
644 carried out prior to CMAP measurement. Stimulation of the sciatic nerve was achieved by
645 placing stimulating electrodes subcutaneously on either side of the sciatic notch and applying
646 supramaximal stimuli (~70 mA) at a rate of 1 pulse per second with the duration of 0.1 ms,
647 using Isolated Pulse Stimulator Model 2100 (A-M Systems). Recording electrode was placed
648 carefully on the GA muscle subdermally without puncturing the muscle, with the reference
649 electrode placed near the Achilles tendon and ground electrode placed on the tail for data
650 recording using Data Recorder IX-RA-834 (iWorx). CMAP amplitude was determined by the
651 absolute difference between potentials of positive and negative peaks, and CMAP latency was

652 determined by the delay from stimulus peak to the beginning of response peak. Three individual
653 measurements were taken from each animal's GA muscle, and average values were used as
654 representatives for statistical analysis.

655

656 ***Toluidine blue staining of sciatic nerves***

657 Sciatic nerve distal to the injury site was dissected at 6 weeks post injury for analysis. The
658 dissected nerves were fixed in 4% paraformaldehyde dissolved in Sorensen's phosphate buffer
659 (0.1M, pH 7.2) at 4°C overnight, followed by procedures described previously (Kim, et al.,
660 2022) with minor modifications for semi-thin sectioning. Briefly, fixed samples were washed
661 with 0.1M sodium cacodylate buffer (pH 7.2), post-fixed with 1% osmium tetroxide in 0.1M
662 sodium cacodylate buffer (pH 7.2) for 1 hour at RT, washed with distilled water (DW) and
663 stained with 0.5% uranyl acetate at 4°C overnight. Stained samples were then washed with DW
664 and dehydrated using serial ethanol and propylene oxide. Samples were then embedded in
665 Spurr's resin (Electron Microscopy Sciences), and semi-thin sections (500 nm) were prepared
666 with a diamond knife on an ultramictorome EM UC7 (Leica). The sections were dried down
667 on glass slides for staining and light microscopy. Toluidine blue staining were done using 1%
668 toluidine blue solution containing 1% sodium borate on a slide warmer (70°C), and images
669 were obtained with the light microscope EVOS FL Auto 2 (Thermo Fisher Scientific) for
670 analysis.

671

672 ***G-ratio quantification***

673 Semi-automated quantification of naked and myelinated axon diameters were carried out using

674 an ImageJ plugin for g-ratio quantification (Goebbels, et al., 2010), where axon diameters and
675 G-ratios were quantified and calculated, respectively. G-ratios were calculated as [naked axon
676 diameter]/[myelinated axon diameter].

677

678 ***Quantification and statistical analysis***

679 All statistical analyses were performed using Prism v5.01 (GraphPad) and R v4.2.1.
680 Continuous variables were tested for normal distribution with Shapiro-Wilk test, and F-test was
681 used to check for equal variance. For comparison of significant differences in multiple groups,
682 one-way analysis of variance(ANOVA) followed by Bonferroni's pairwise post hoc test was
683 applied. For comparison of two groups, unpaired t-test was used for data with normal
684 distribution and equal variance; Welch's t-test was used for data with normal distribution and
685 unequal variance; and Mann-Whitney U test was used for non-normally distributed data.
686 ANCOVA was applied to test for differences between slopes of linear regression lines. Two-
687 way ANOVA was applied to compare two groups with two variables. For comparison of gene
688 expression levels between scRNA-seq data, Wilcoxon rank sum test was applied as a default
689 in functions FindAllMarkers and FindMarkers within the R package Seurat v4.3.0. For RT-
690 qPCR, the average of triplicate technical values were used for each biological replicate. All
691 error bars represent mean ± SD. P value of less than 0.05 was considered statistically significant
692 at the 95% confidence level. The number of technical and biological replicates and statistical
693 analysis used in each experiment are indicated in the figure legends.

694

695 **Data availability**

696 Single-cell RNA-sequencing data produced in this study have been deposited at GEO under
697 accession number GSE250436 and are publicly available as of the date of publication.

698

699 **Acknowledgments**

700 We thank Dr. Jong-Eun Park for his helpful comments on the analysis of our scRNA-seq data.
701 *Prrx1*$^{Cre}$ mice, *Bdnf*$^{fl}$ mice, and *Plp1*$^{CreER}$ mice were obtained via Korea Mouse Phenotyping
702 Center, deposited by Dr. Rho Hyun Seong, Dr. Yun-Hee Lee, and Dr. Myunghwan Choi,
703 respectively. Also, we would like to acknowledge technical support from Center for Research
704 Facilities, Biological Sciences Department, Seoul National University (SNU) and SNU
705 National Instrumentation Center for Environmental Management. Library construction and
706 sequencing of the scRNA-seq data was performed by Macrogen Inc.. Experimental schemes
707 and graphical summary in this paper were created using BioRender. This work was supported
708 by grants from the National Research Foundation of Korea (NRF-2020R1A5A1018081, NRF-
709 2022R1A2C3007621) funded by the Korean government (MSIT).

710

711 **References**

712 Airaksinen MS, Saarma M (2002) **The GDNF family: signalling, biological functions and**
713 **therapeutic value** *Nat Rev Neurosci* 3:383-94.10.1038/nrn812

714

715 Arthur-Farraj PJ, Latouche M, Wilton DK, Quintes S, Chabrol E, Banerjee A, Woodhoo A,
716 Jenkins B, Rahman M, Turmaine M, Wicher GK, Mitter R, Greensmith L, Behrens A, Raivich
717 G, Mirsky R, Jessen KR (2012) **c-Jun reprograms Schwann cells of injured nerves to**
718 **generate a repair cell essential for regeneration** *Neuron* 75:633-
719 47.10.1016/j.neuron.2012.06.021

720

721 Aurora AB, Olson EN (2014) **Immune modulation of stem cells and regeneration** *Cell Stem*

722 *Cell* 15:14-25.10.1016/j.stem.2014.06.009

723

724 Bakooshli MA, Wang YX, Monti E, Su S, Kraft P, Nalbandian M, Alexandrova L, Wheeler JR,
725 Vogel H, Blau HM (2023) **Regeneration of neuromuscular synapses after acute and chronic**
726 **denervation by inhibiting the gerozyme 15-prostaglandin dehydrogenase** *Science*
727 *Translational Medicine* 15:eadg1485.doi:10.1126/scitranslmed.adg1485

728

729 Baydyuk M, Xu B (2014) **BDNF signaling and survival of striatal neurons** *Front Cell*
730 *Neurosci* 8:254.10.3389/fncel.2014.00254

731

732 Buttner R, Schulz A, Reuter M, Akula AK, Mindos T, Carlstedt A, Riecken LB, Baader SL,
733 Bauer R, Morrison H (2018) **Inflammaging impairs peripheral nerve maintenance and**
734 **regeneration** *Aging Cell* 17:e12833.10.1111/acel.12833

735

736 Carr MJ, Toma JS, Johnston APW, Steadman PE, Yuzwa SA, Mahmud N, Frankland PW,
737 Kaplan DR, Miller FD (2019) **Mesenchymal Precursor Cells in Adult Nerves Contribute to**
738 **Mammalian Tissue Repair and Regeneration** *Cell Stem Cell* 24:240-256
739 e9.10.1016/j.stem.2018.10.024

740

741 Chung T, Prasad K, Lloyd TE (2014) **Peripheral neuropathy: clinical and**
742 **electrophysiological considerations** *Neuroimaging Clin N Am* 24:49-
743 65.10.1016/j.nic.2013.03.023

744

745 Contreras O, Rebolledo DL, Oyarzun JE, Olguin HC, Brandan E (2016) **Connective tissue**
746 **cells expressing fibro/adipogenic progenitor markers increase under chronic damage:**
747 **relevance in fibroblast-myofibroblast differentiation and skeletal muscle fibrosis** *Cell*
748 *Tissue Res* 364:647-660.10.1007/s00441-015-2343-0

749

750 Contreras O, Rossi FMV, Theret M (2021) **Origins, potency, and heterogeneity of skeletal**
751 **muscle fibro-adipogenic progenitors-time for new definitions** *Skelet Muscle*
752 11:16.10.1186/s13395-021-00265-6

753

754 De Micheli AJ, Laurilliard EJ, Heinke CL, Ravichandran H, Fraczek P, Soueid-Baumgarten S,
755 De Vlaminck I, Elemento O, Cosgrove BD (2020) **Single-Cell Analysis of the Muscle Stem**
756 **Cell Hierarchy Identifies Heterotypic Communication Signals Involved in Skeletal**
757 **Muscle Regeneration** *Cell Rep* 30:3583-3595 e5.10.1016/j.celrep.2020.02.067

758

759 Doerflinger NH, Macklin WB, Popko B (2003) **Inducible site-specific recombination in**
760 **myelinating cells** *Genesis* 35:63-72.10.1002/gene.10154

761

762 English AW, Liu K, Nicolini JM, Mulligan AM, Ye K (2013) **Small-molecule trkB agonists**

**promote axon regeneration in cut peripheral nerves** *Proc Natl Acad Sci U S A* 110:16217-22.10.1073/pnas.1303646110

Fielder GC, Yang TW, Razdan M, Li Y, Lu J, Perry JK, Lobie PE, Liu DX (2018) **The GDNF Family: A Role in Cancer?** *Neoplasia* 20:99-117.10.1016/j.neo.2017.10.010

Forese MG, Pellegatta M, Canevazzi P, Gullotta GS, Podini P, Rivellini C, Previtali SC, Bacigaluppi M, Quattrini A, Taveggia C (2020) **Prostaglandin D2 synthase modulates macrophage activity and accumulation in injured peripheral nerves** *Glia* 68:95-110.10.1002/glia.23705

Ghosh A, Carnahan J, Greenberg ME (1994) **Requirement for BDNF in activity-dependent survival of cortical neurons** *Science* 263:1618-1623.10.1126/science.7907431

Goebbels S, Oltrogge JH, Kemper R, Heilmann I, Bormuth I, Wolfer S, Wichert SP, Mobius W, Liu X, Lappe-Siefke C, Rossner MJ, Groszer M, Suter U, Frahm J, Boretius S, Nave KA (2010) **Elevated phosphatidylinositol 3,4,5-trisphosphate in glia triggers cell-autonomous membrane wrapping and myelination** *J Neurosci* 30:8953-64.10.1523/JNEUROSCI.0219-10.2010

Gonzalez D, Contreras O, Rebolledo DL, Espinoza JP, van Zundert B, Brandan E (2017) **ALS skeletal muscle shows enhanced TGF-beta signaling, fibrosis and induction of fibro/adipogenic progenitor markers** *PLoS One* 12:e0177649.10.1371/journal.pone.0177649

Grinsell D, Keating CP (2014) **Peripheral nerve reconstruction after injury: a review of clinical and experimental therapies** *Biomed Res Int* 2014:698256.10.1155/2014/698256

Hammarberg H, Piehl F, Cullheim S, Fjell J, Hokfelt T, Fried K (1996) **GDNF mRNA in Schwann cells and DRG satellite cells after chronic sciatic nerve injury** *NeuroReport* 7:857-860.10.1097/00001756-199603220-00004

Han H, Cho JW, Lee S, Yun A, Kim H, Bae D, Yang S, Kim CY, Lee M, Kim E, Lee S, Kang B, Jeong D, Kim Y, Jeon HN, Jung H, Nam S, Chung M, Kim JH, Lee I (2018) **TRRUST v2: an expanded reference database of human and mouse transcriptional regulatory interactions** *Nucleic Acids Res* 46:D380-D386.10.1093/nar/gkx1013

Hann S-H, Kim S-Y, Kim Y-L, Jo Y-W, Kang J-S, Park H, Choi S-Y, Kong Y-Y (2023) **Depletion of SMN Protein in Mesenchymal Progenitors Impairs the Development of Bone and Neuromuscular Junction in Spinal Muscular Atrophy** *eLife Sciences Publications, Ltd* 10.7554/elife.92731.1

Hanz S, Perlson E, Willis D, Zheng JQ, Massarwa R, Huerta JJ, Koltzenburg M, Kohler M,

van-Minnen J, Twiss JL, Fainzilber M (2003) **Axoplasmic importins enable retrograde injury signaling in lesioned nerve** *Neuron* 40:1095-1104.10.1016/s0896-6273(03)00770-0

Hao Y, Hao S, Andersen-Nissen E, Mauck WM, 3rd, Zheng S, Butler A, Lee MJ, Wilk AJ, Darby C, Zager M, Hoffman P, Stoeckius M, Papalexi E, Mimitou EP, Jain J, Srivastava A, Stuart T, Fleming LM, Yeung B, Rogers AJ, McElrath JM, Blish CA, Gottardo R, Smibert P, Satija R (2021) **Integrated analysis of multimodal single-cell data** *Cell* 184:3573-3587 e29.10.1016/j.cell.2021.04.048

Heredia JE, Mukundan L, Chen FM, Mueller AA, Deo RC, Locksley RM, Rando TA, Chawla A (2013) **Type 2 innate signals stimulate fibro/adipogenic progenitors to facilitate muscle regeneration** *Cell* 153:376-88.10.1016/j.cell.2013.02.053

Hoke A, Gordon T, Zochodne DW, Sulaiman OA (2002) **A decline in glial cell-line-derived neurotrophic factor expression is associated with impaired regeneration after long-term Schwann cell denervation** *Exp Neurol* 173:77-85.10.1006/exnr.2001.7826

Jing S, Wen D, Yu Y, Holst PL, Luo Y, Fang M, Tamir R, Antonio L, Hu Z, Cupples R (1996) **GDNF–induced activation of the ret protein tyrosine kinase is mediated by GDNFR-α, a novel receptor for GDNF** *Cell* 85:1113-1124.
Joe AW, Yi L, Natarajan A, Le Grand F, So L, Wang J, Rudnicki MA, Rossi FM (2010) **Muscle injury activates resident fibro/adipogenic progenitors that facilitate myogenesis** *Nat Cell Biol* 12:153-63.10.1038/ncb2015

Joseph NM, Mukouyama YS, Mosher JT, Jaegle M, Crone SA, Dormand EL, Lee KF, Meijer D, Anderson DJ, Morrison SJ (2004) **Neural crest stem cells undergo multilineage differentiation in developing peripheral nerves to generate endoneurial fibroblasts in addition to Schwann cells** *Development* 131:5599-612.10.1242/dev.01429

Julier Z, Park AJ, Briquez PS, Martino MM (2017) **Promoting tissue regeneration by modulating the immune system** *Acta Biomater* 53:13-28.10.1016/j.actbio.2017.01.056

Kalinski AL, Yoon C, Huffman LD, Duncker PC, Kohen R, Passino R, Hafner H, Johnson C, Kawaguchi R, Carbajal KS, Jara JS, Hollis E, Geschwind DH, Segal BM, Giger RJ (2020) **Analysis of the immune response to sciatic nerve injury identifies efferocytosis as a key mechanism of nerve debridement** *Elife* 9:10.7554/eLife.60223

Kanehisa M, Furumichi M, Sato Y, Kawashima M, Ishiguro-Watanabe M (2023) **KEGG for taxonomy-based analysis of pathways and genomes** *Nucleic Acids Res* 51:D587-D592.10.1093/nar/gkac963

Kim JH, Kang JS, Yoo K, Jeong J, Park I, Park JH, Rhee J, Jeon S, Jo YW, Hann SH, Seo M,

Moon S, Um SJ, Seong RH, Kong YY (2022) **Bap1/SMN axis in Dpp4+ skeletal muscle mesenchymal cells regulates the neuromuscular system** *JCI Insight* 7:10.1172/jci.insight.158380

Kolberg L, Raudvere U, Kuzmin I, Adler P, Vilo J, Peterson H (2023) **g:Profiler-interoperable web service for functional enrichment analysis and gene identifier mapping (2023 update)** *Nucleic Acids Res* 51:W207-W212.10.1093/nar/gkad347

Kucera M, Isserlin R, Arkhangorodsky A, Bader GD (2016) **AutoAnnotate: A Cytoscape app for summarizing networks with semantic annotations** *F1000Res* 5:1717.10.12688/f1000research.9090.1

La Manno G, Soldatov R, Zeisel A, Braun E, Hochgerner H, Petukhov V, Lidschreiber K, Kastriti ME, Lonnerberg P, Furlan A, Fan J, Borm LE, Liu Z, van Bruggen D, Guo J, He X, Barker R, Sundstrom E, Castelo-Branco G, Cramer P, Adameyko I, Linnarsson S, Kharchenko PV (2018) **RNA velocity of single cells** *Nature* 560:494-498.10.1038/s41586-018-0414-6

Leinroth AP, Mirando AJ, Rouse D, Kobayahsi Y, Tata PR, Rueckert HE, Liao Y, Long JT, Chakkalakal JV, Hilton MJ (2022) **Identification of distinct non-myogenic skeletal-muscle-resident mesenchymal cell populations** *Cell Rep* 39:110785.10.1016/j.celrep.2022.110785

Lemos DR, Babaeijandaghi F, Low M, Chang CK, Lee ST, Fiore D, Zhang RH, Natarajan A, Nedospasov SA, Rossi FM (2015) **Nilotinib reduces muscle fibrosis in chronic muscle injury by promoting TNF-mediated apoptosis of fibro/adipogenic progenitors** *Nat Med* 21:786-94.10.1038/nm.3869

Lieberman B, Kusi M, Hung CN, Chou CW, He N, Ho YY, Taverna JA, Huang THM, Chen CL (2021) **Toward uncharted territory of cellular heterogeneity: advances and applications of single-cell RNA-seq** *J Transl Genet Genom* 5:1-21.10.20517/jtgg.2020.51

Lin H, Ma X, Sun Y, Peng H, Wang Y, Thomas SS, Hu Z (2022) **Decoding the transcriptome of denervated muscle at single-nucleus resolution** *J Cachexia Sarcopenia Muscle* 13:2102-2117.10.1002/jcsm.13023

Liu L, Cheung TH, Charville GW, Rando TA (2015) **Isolation of skeletal muscle stem cells by fluorescence-activated cell sorting** *Nat Protoc* 10:1612-24.10.1038/nprot.2015.110

Logan M, Martin JF, Nagy A, Lobe C, Olson EN, Tabin CJ (2002) **Expression of Cre Recombinase in the developing mouse limb bud driven by a Prxl enhancer** *Genesis* 33:77-80.10.1002/gene.10092

Lukjanenko L, Karaz S, Stuelsatz P, Gurriaran-Rodriguez U, Michaud J, Dammone G, Sizzano F, Mashinchian O, Ancel S, Migliavacca E, Liot S, Jacot G, Metairon S, Raymond F, Descombes P, Palini A, Chazaud B, Rudnicki MA, Bentzinger CF, Feige JN (2019) **Aging Disrupts Muscle Stem Cell Function by Impairing Matricellular WISP1 Secretion from Fibro-Adipogenic Progenitors** *Cell Stem Cell* 24:433-446 e7.10.1016/j.stem.2018.12.014

Madaro L, Passafaro M, Sala D, Etxaniz U, Lugarini F, Proietti D, Alfonsi MV, Nicoletti C, Gatto S, De Bardi M, Rojas-Garcia R, Giordani L, Marinelli S, Pagliarini V, Sette C, Sacco A, Puri PL (2018) **Denervation-activated STAT3-IL-6 signalling in fibro-adipogenic progenitors promotes myofibres atrophy and fibrosis** *Nat Cell Biol* 20:917-927.10.1038/s41556-018-0151-y

Magill CK, Tong A, Kawamura D, Hayashi A, Hunter DA, Parsadanian A, Mackinnon SE, Myckatyn TM (2007) **Reinnervation of the tibialis anterior following sciatic nerve crush injury: a confocal microscopic study in transgenic mice** *Exp Neurol* 207:64-74.10.1016/j.expneurol.2007.05.028

Maita KC, Garcia JP, Avila FR, Torres-Guzman RA, Ho O, Chini CCS, Chini EN, Forte AJ (2023) **Evaluation of the Aging Effect on Peripheral Nerve Regeneration: A Systematic Review** *J Surg Res* 288:329-340.10.1016/j.jss.2023.03.017

Malecova B, Gatto S, Etxaniz U, Passafaro M, Cortez A, Nicoletti C, Giordani L, Torcinaro A, De Bardi M, Bicciato S, De Santa F, Madaro L, Puri PL (2018) **Dynamics of cellular states of fibro-adipogenic progenitors during myogenesis and muscular dystrophy** *Nat Commun* 9:3670.10.1038/s41467-018-06068-6

Mallik A, Weir AI (2005) **Nerve conduction studies: essentials and pitfalls in practice** *J Neurol Neurosurg Psychiatry* 76 Suppl 2:ii23-31.10.1136/jnnp.2005.069138

Merico D, Isserlin R, Stueker O, Emili A, Bader GD (2010) **Enrichment map: a network-based method for gene-set enrichment visualization and interpretation** *PLoS One* 5:e13984.10.1371/journal.pone.0013984

Mueller M, Wacker K, Ringelstein EB, Hickey WF, Imai Y, Kiefer R (2001) **Rapid response of identified resident endoneurial macrophages to nerve injury** *Am J Pathol* 159:2187-97.10.1016/S0002-9440(10)63070-2

Murphy MM, Lawson JA, Mathew SJ, Hutcheson DA, Kardon G (2011) **Satellite cells, connective tissue fibroblasts and their interactions are crucial for muscle regeneration** *Development* 138:3625-37.10.1242/dev.064162

Nicoletti C, Wei X, Etxaniz U, D'Ercole C, Madaro L, Perera R, Puri PL (2023) **Muscle**

**denervation promotes functional interactions between glial and mesenchymal cells through NGFR and NGF** *iScience* 26:107114.10.1016/j.isci.2023.107114

Nicoletti C, Wei X, Etxaniz U, Proietti D, Madaro L, Puri PL (2020) **scRNA-seq-based analysis of skeletal muscle response to denervation reveals selective activation of muscle-resident glial cells and fibroblasts** *Biorxiv* 10.1101/2020.12.29.424762

Oprescu SN, Yue F, Qiu J, Brito LF, Kuang S (2020) **Temporal Dynamics and Heterogeneity of Cell Populations during Skeletal Muscle Regeneration** *iScience* 23:100993.10.1016/j.isci.2020.100993

Ortega-Gomez A, Perretti M, Soehnlein O (2013) **Resolution of inflammation: an integrated view** *EMBO Mol Med* 5:661-74.10.1002/emmm.201202382

Oudega M, Hagg T (1999) **Neurotrophins promote regeneration of sensory axons in the adult rat spinal cord** *Brain Research* 818:431-438.

Painter MW, Brosius Lutz A, Cheng YC, Latremoliere A, Duong K, Miller CM, Posada S, Cobos EJ, Zhang AX, Wagers AJ, Havton LA, Barres B, Omura T, Woolf CJ (2014) **Diminished Schwann cell repair responses underlie age-associated impaired axonal regeneration** *Neuron* 83:331-343.10.1016/j.neuron.2014.06.016

Parrinello S, Napoli I, Ribeiro S, Wingfield Digby P, Fedorova M, Parkinson DB, Doddrell RD, Nakayama M, Adams RH, Lloyd AC (2010) **EphB signaling directs peripheral nerve regeneration through Sox2-dependent Schwann cell sorting** *Cell* 143:145-55.10.1016/j.cell.2010.08.039

Proietti D, Giordani L, De Bardi M, D'Ercole C, Lozanoska-Ochser B, Amadio S, Volonte C, Marinelli S, Muchir A, Bouche M, Borsellino G, Sacco A, Puri PL, Madaro L (2021) **Activation of skeletal muscle-resident glial cells upon nerve injury** *JCI Insight* 6:10.1172/jci.insight.143469

Reimand J, Isserlin R, Voisin V, Kucera M, Tannus-Lopes C, Rostamianfar A, Wadi L, Meyer M, Wong J, Xu C, Merico D, Bader GD (2019) **Pathway enrichment analysis and visualization of omics data using g:Profiler, GSEA, Cytoscape and EnrichmentMap** *Nat Protoc* 14:482-517.10.1038/s41596-018-0103-9

Roberts EW, Deonarine A, Jones JO, Denton AE, Feig C, Lyons SK, Espeli M, Kraman M, McKenna B, Wells RJ, Zhao Q, Caballero OL, Larder R, Coll AP, O'Rahilly S, Brindle KM, Teichmann SA, Tuveson DA, Fearon DT (2013) **Depletion of stromal cells expressing fibroblast activation protein-alpha from skeletal muscle and bone marrow results in cachexia and anemia** *J Exp Med* 210:1137-51.10.1084/jem.20122344

Saito Y, Chikenji TS, Matsumura T, Nakano M, Fujimiya M (2020) **Exercise enhances skeletal muscle regeneration by promoting senescence in fibro-adipogenic progenitors** *Nat Commun* 11:889.10.1038/s41467-020-14734-x

Sariola H, Saarma M (2003) **Novel functions and signalling pathways for GDNF** *J Cell Sci* 116:3855-62.10.1242/jcs.00786

Scheib J, Hoke A (2013) **Advances in peripheral nerve regeneration** *Nat Rev Neurol* 9:668-76.10.1038/nrneurol.2013.227

Scheib JL, Hoke A (2016) **An attenuated immune response by Schwann cells and macrophages inhibits nerve regeneration in aged rats** *Neurobiol Aging* 45:1-9.10.1016/j.neurobiolaging.2016.05.004

Scott RW, Arostegui M, Schweitzer R, Rossi FMV, Underhill TM (2019) **Hic1 Defines Quiescent Mesenchymal Progenitor Subpopulations with Distinct Functions and Fates in Skeletal Muscle Regeneration** *Cell Stem Cell* 25:797-813 e9.10.1016/j.stem.2019.11.004

Shannon P, Markiel A, Ozier O, Baliga NS, Wang JT, Ramage D, Amin N, Schwikowski B, Ideker T (2003) **Cytoscape: a software environment for integrated models of biomolecular interaction networks** *Genome Res* 13:2498-504.10.1101/gr.1239303

Takemura Y, Imai S, Kojima H, Katagi M, Yamakawa I, Kasahara T, Urabe H, Terashima T, Yasuda H, Chan L, Kimura H, Matsusue Y (2012) **Brain-derived neurotrophic factor from bone marrow-derived cells promotes post-injury repair of peripheral nerve** *PLoS One* 7:e44592.10.1371/journal.pone.0044592

Theret M, Rossi FMV, Contreras O (2021) **Evolving Roles of Muscle-Resident Fibro-Adipogenic Progenitors in Health, Regeneration, Neuromuscular Disorders, and Aging** *Front Physiol* 12:673404.10.3389/fphys.2021.673404

Toma JS, Karamboulas K, Carr MJ, Kolaj A, Yuzwa SA, Mahmud N, Storer MA, Kaplan DR, Miller FD (2020) **Peripheral Nerve Single-Cell Analysis Identifies Mesenchymal Ligands that Promote Axonal Growth** *eNeuro* 7:10.1523/ENEURO.0066-20.2020

Treanor JJ, Goodman L, de Sauvage F, Stone DM, Poulsen KT, Beck CD, Gray C, Armanini MP, Pollock RA, Hefti F (1996) **Characterization of a multicomponent receptor for GDNF** *Nature* 382:80-83.

Trupp M, Arenas E, Fainzilber M, Nilsson AS, Sieber BA, Grigoriou M, Kilkenny C, Salazar-Grueso E, Pachnis V, Arumae U, Sariola H, Saarma M, Ibanez CF (1996) **Functional receptor for GDNF encoded by the c-ret proto-oncogene** *Nature* 381:785-789.10.1038/381785a0

Uezumi A, Fukada S, Yamamoto N, Takeda S, Tsuchida K (2010) **Mesenchymal progenitors distinct from satellite cells contribute to ectopic fat cell formation in skeletal muscle** *Nat Cell Biol* 12:143-52.10.1038/ncb2014

Uezumi A, Ikemoto-Uezumi M, Tsuchida K (2014) **Roles of nonmyogenic mesenchymal progenitors in pathogenesis and regeneration of skeletal muscle** *Front Physiol* 5:68.10.3389/fphys.2014.00068

Uezumi A, Ikemoto-Uezumi M, Zhou H, Kurosawa T, Yoshimoto Y, Nakatani M, Hitachi K, Yamaguchi H, Wakatsuki S, Araki T, Morita M, Yamada H, Toyoda M, Kanazawa N, Nakazawa T, Hino J, Fukada SI, Tsuchida K (2021) **Mesenchymal Bmp3b expression maintains skeletal muscle integrity and decreases in age-related sarcopenia** *J Clin Invest* 131:10.1172/JCI139617

Uezumi A, Ito T, Morikawa D, Shimizu N, Yoneda T, Segawa M, Yamaguchi M, Ogawa R, Matev MM, Miyagoe-Suzuki Y, Takeda S, Tsujikawa K, Tsuchida K, Yamamoto H, Fukada S (2011) **Fibrosis and adipogenesis originate from a common mesenchymal progenitor in skeletal muscle** *J Cell Sci* 124:3654-64.10.1242/jcs.086629

Vallecillo-Garcia P, Orgeur M, Vom Hofe-Schneider S, Stumm J, Kappert V, Ibrahim DM, Borno ST, Hayashi S, Relaix F, Hildebrandt K, Sengle G, Koch M, Timmermann B, Marazzi G, Sassoon DA, Duprez D, Stricker S (2017) **Odd skipped-related 1 identifies a population of embryonic fibro-adipogenic progenitors regulating myogenesis during limb development** *Nat Commun* 8:1218.10.1038/s41467-017-01120-3

Verdú E, Ceballos D, Vilches JJ, Navarro X (2008) **Influence of aging on peripheral nerve function and regeneration** *Journal of the Peripheral Nervous System* 5:191-208.10.1111/j.1529-8027.2000.00026.x

Wagstaff LJ, Gomez-Sanchez JA, Fazal SV, Otto GW, Kilpatrick AM, Michael K, Wong LYN, Ma KH, Turmaine M, Svaren J, Gordon T, Arthur-Farraj P, Velasco-Aviles S, Cabedo H, Benito C, Mirsky R, Jessen KR (2021) **Failures of nerve regeneration caused by aging or chronic denervation are rescued by restoring Schwann cell c-Jun** *Elife* 10:10.7554/eLife.62232

Wilhelm JC, Xu M, Cucoranu D, Chmielewski S, Holmes T, Lau KS, Bassell GJ, English AW (2012) **Cooperative roles of BDNF expression in neurons and Schwann cells are modulated by exercise to facilitate nerve regeneration** *J Neurosci* 32:5002-9.10.1523/JNEUROSCI.1411-11.2012

Wosczyna MN, Konishi CT, Perez Carbajal EE, Wang TT, Walsh RA, Gan Q, Wagner MW, Rando TA (2019) **Mesenchymal Stromal Cells Are Required for Regeneration and**

1055 **Homeostatic Maintenance of Skeletal Muscle** *Cell Rep* 27:2029-2035
1056 e5.10.1016/j.celrep.2019.04.074

1057
1058 Xiao J, Wong AW, Willingham MM, Kaasinen SK, Hendry IA, Howitt J, Putz U, Barrett GL,
1059 Kilpatrick TJ, Murray SS (2009) **BDNF exerts contrasting effects on peripheral myelination**
1060 **of NGF-dependent and BDNF-dependent DRG neurons** *J Neurosci* 29:4016-
1061 22.10.1523/JNEUROSCI.3811-08.2009

1062
1063 Xu P, Rosen KM, Hedstrom K, Rey O, Guha S, Hart C, Corfas G (2013) **Nerve injury induces**
1064 **glial cell line-derived neurotrophic factor (GDNF) expression in Schwann cells through**
1065 **purinergic signaling and the PKC-PKD pathway** *Glia* 61:1029-40.10.1002/glia.22491

1066
1067 Zhang JY, Luo XG, Xian CJ, Liu ZH, Zhou XF (2000) **Endogenous BDNF is required for**
1068 **myelination and regeneration of injured sciatic nerve in rodents** *European Journal of*
1069 *Neuroscience* 12:4171-4180.10.1111/j.1460-9568.2000.01312.x

1070
1071 Zheng J, Sun J, Lu X, Zhao P, Li K, Li L (2016) **BDNF promotes the axonal regrowth after**
1072 **sciatic nerve crush through intrinsic neuronal capability upregulation and distal portion**
1073 **protection** *Neurosci Lett* 621:1-8.10.1016/j.neulet.2016.04.006

1074

1075

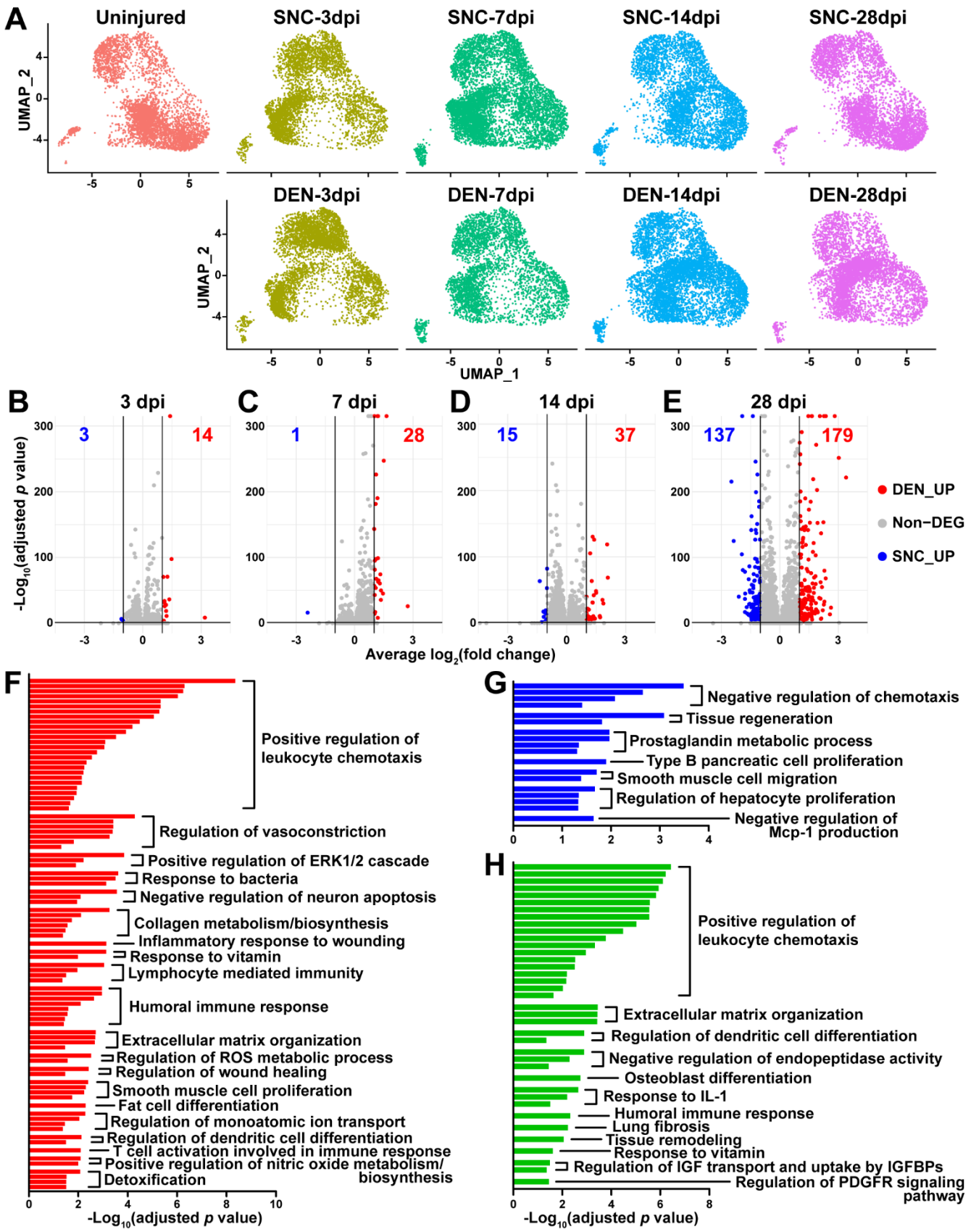


**Figure 1. Distinct response profiles of FAPs upon nerve crush injury versus denervation.**
(**A**) Single-cell transcriptome data of nerve injury-affected FAPs displayed separately by samples on UMAP plots. (**B**–**E**) Volcano plots showing different numbers of DEGs identified from comparing SNC- vs DEN-affected FAPs at (B) 3, (C) 7, (D) 14, (E) 28 days post injury (dpi). (**F**–**H**) Pathway terms enriched from gene set overrepresentation analyses using g:Profiler. DEGs used as input were (F) DEN-28dpi-upregulated versus SNC-28dpi, (G) SNC-28dpi-upregulated versus DEN-28dpi, and (H) DEGs upregulated commonly in SNC-3dpi, SNC-7dpi, DEN-3dpi, and DEN-7dpi versus uninjured control.

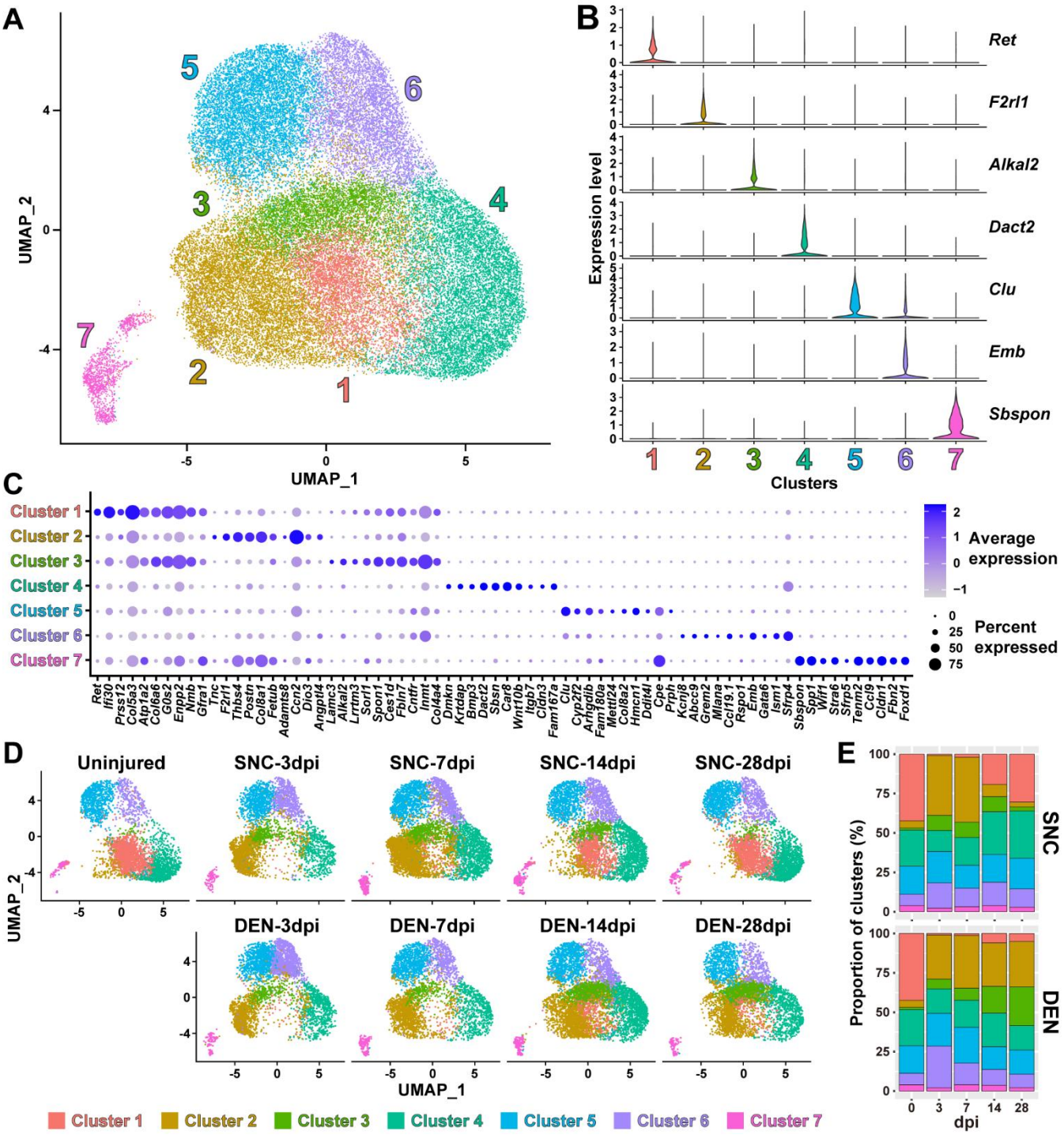


**Figure 2. Nerve injury-responsive subsets within FAPs.**
(**A**) Seven clusters identified by unsupervised clustering using all nine scRNA-seq samples obtained in this study displayed on the UMAP plot. (**B**) Violin plots showing expressions of unique marker genes identified in each cluster. (**C**) Dotplot showing the expression levels and percentages of top 10 DEGs enriched in each cluster. (**D**) UMAP plots of clustered scRNA-seq data displayed separately by samples. (**E**) Barplots showing the proportions of the seven clusters that comprise each scRNA-seq sample of nerve injury-affected FAPs. For 0 dpi, data from the same uninjured control sample is displayed for both SNC and DEN.

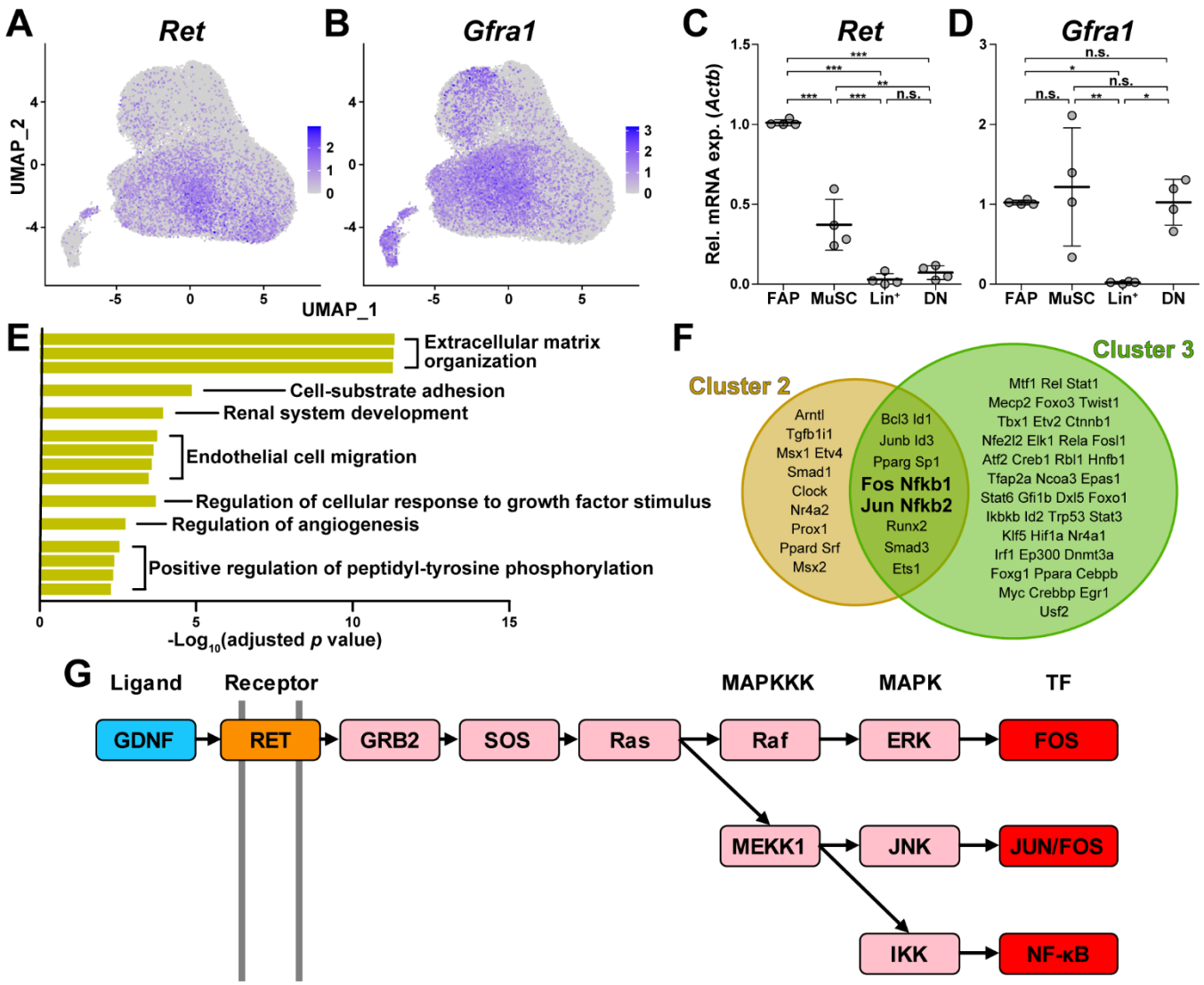


**Figure 3. GDNF signaling pathway in the nerve injury-sensing mechanism by FAPs.**
(**A**–**B**) UMAP plots showing the expressions of (A) *Ret* and (B) *Gfra1* in the merged scRNA-seq data. (**C**–**D**) RT-qPCR results showing the expressions of (C) *Ret* and (D) *Gfra1* in mononuclear cells isolated from uninjured muscles by FACS. MuSC, muscle stem cells; Lin$^+$, lineage-positive cells; DN, Vcam1/Sca1 double-negative cells. n = 4; one-way ANOVA with Bonferroni's post hoc test. * $p < 0.05$, ** $p < 0.01$, *** $p < 0.001$, n.s., not significant. (**E**) Shared pathway terms commonly identified from gene set overrepresentation analyses using DEGs specifically upregulated in clusters 1, 2 or 3. (**F**) Venn diagram showing the results from TRRUST analyses using DEGs enriched in clusters 2 and 3. Transcription factors predicted to regulate genes upregulated in each cluster are listed. (**G**) Simplified diagram of the GDNF signaling pathway. Blue: GDNF ligand; orange: GDNF receptor Ret expressed in cluster 1; pink: downstream cascade genes expressed in clusters 1-3; red: transcription factors commonly predicted to regulate upregulated genes in clusters 2 and 3.

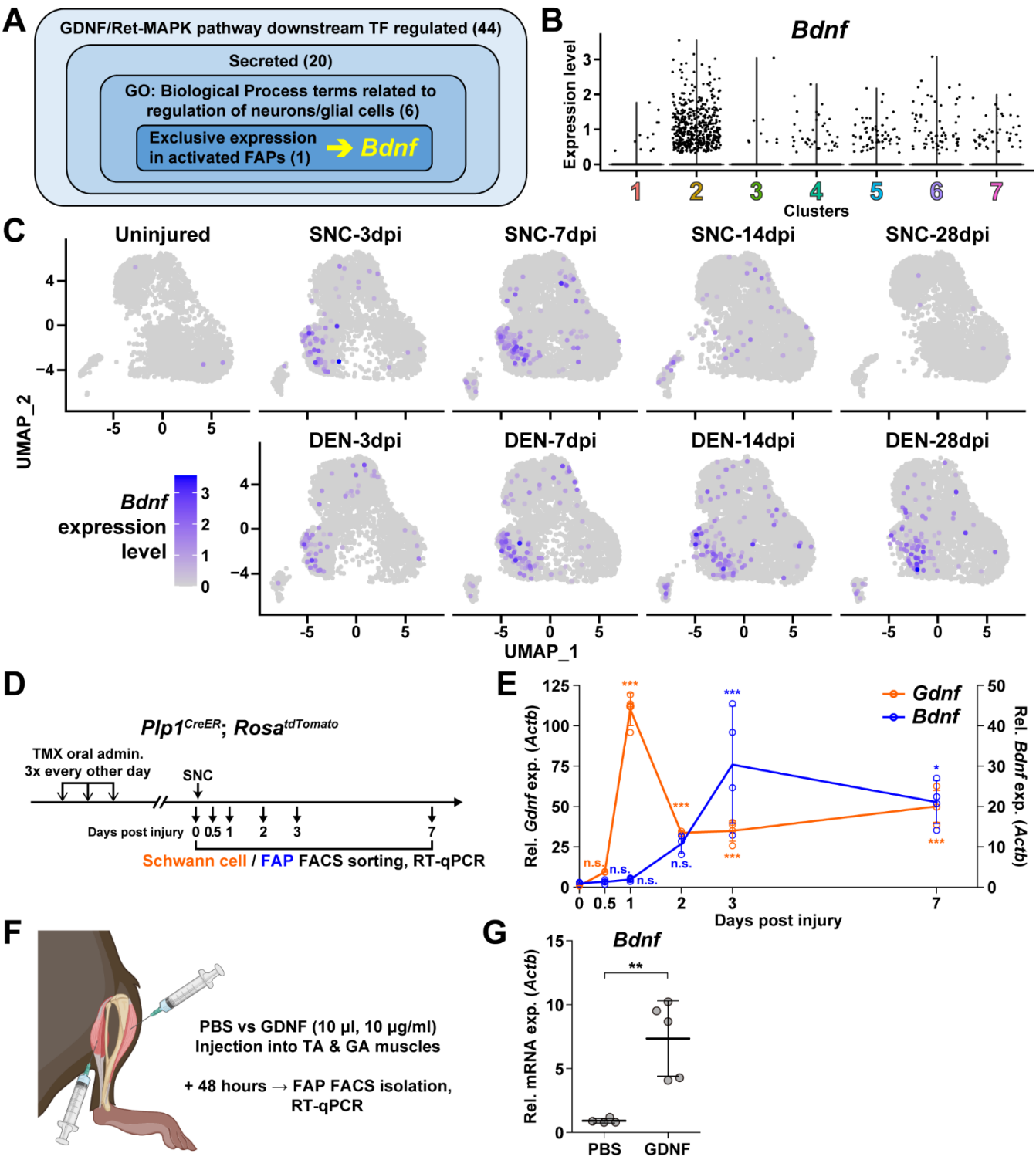


**Figure 4. *Bdnf* expression in FAPs by both endogenous and exogenous GDNF.**
(**A**) Scheme for identification of candidate genes expressed in FAPs in response to GDNF that may contribute to nerve regeneration. Number of genes that fit into each criterion is indicated. (**B**) Violin plot displaying the expression levels of *Bdnf* in the seven clusters. (**C**) Expression of *Bdnf* in each scRNA-seq sample shown on UMAP plots. (**D**) Experimental scheme for sampling Schwann cells and FAPs at different time points post SNC for gene expression analyses. (**E**) RT-qPCR results showing the expression levels of *Gdnf* from Schwann cells (orange dot and line, left y-axis) and *Bdnf* from FAPs (blue dot and line, right y-axis) at different time points post SNC displayed on the same plot. n = 4, except for 0 and 2 dpi, where n = 3. One-way ANOVA with Bonferroni's post hoc test. * $p < 0.05$, *** $p < 0.001$, n.s., not significant. (**F**) Experimental scheme for intramuscular injection of either PBS or recombinant mouse GDNF protein, with the time point for FAP isolation post injection indicated. (**G**) RT-qPCR results showing the expression level of *Bdnf* in FAPs 48 hours post intramuscular injection of either PBS (n = 4) or GDNF (n = 5). Unpaired t-test with Welch's correction. ** $p < 0.01$.

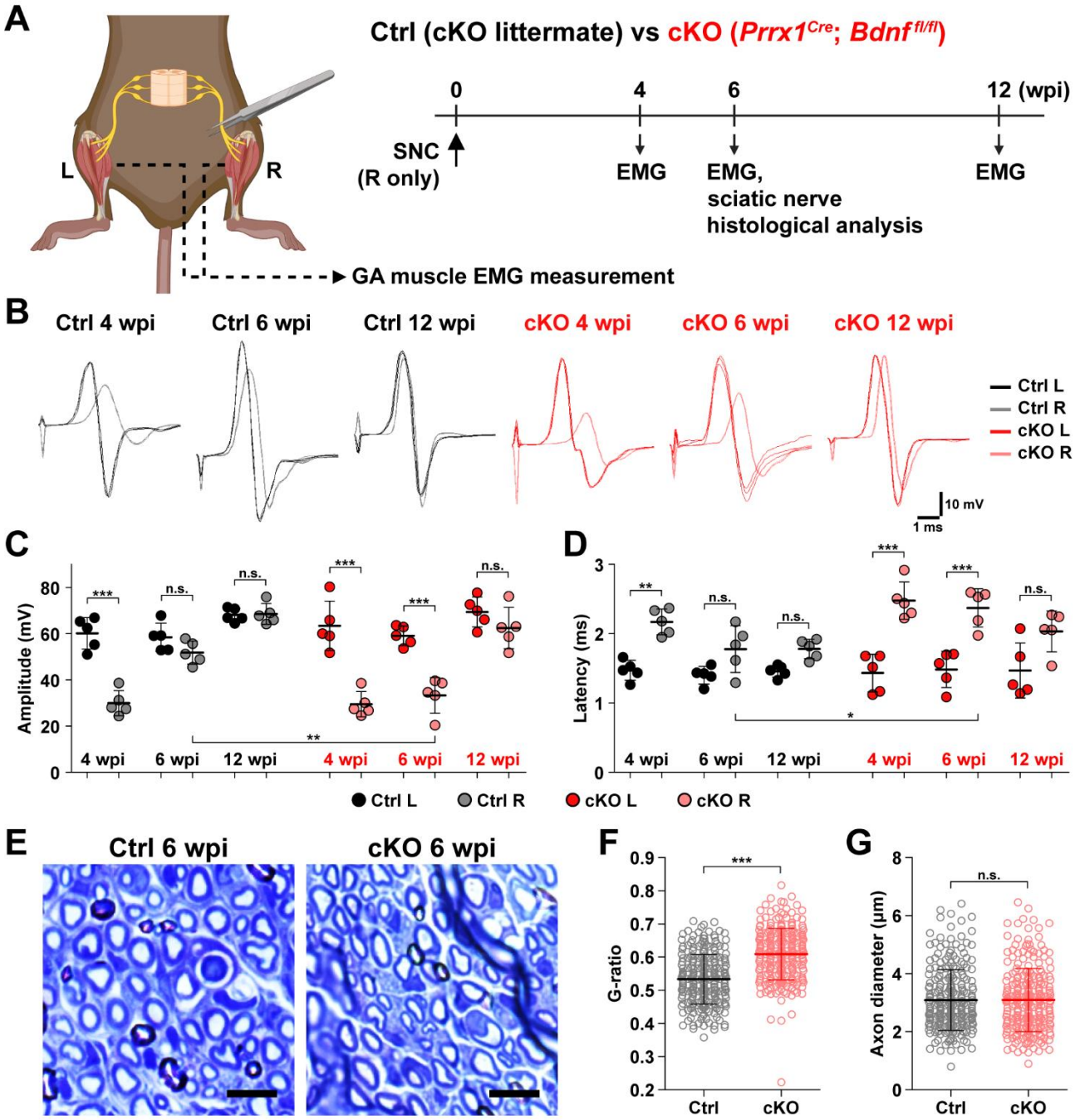


**Figure 5. Remyelination by FAP-derived BDNF during peripheral nerve regeneration.**
(**A**) Experimental scheme displaying mice used and the time points selected for EMG measurements and sciatic nerve dissection. wpi, weeks post injury. (**B**) Representative EMG measurement results of both injured and uninjured GA muscles from Ctrl or cKO mice at the indicated time points post SNC. (**C**–**D**) Quantified results of EMG measurement showing (C) CMAP amplitude and (D) CMAP latency. n = 5. One-way ANOVA with Bonferroni's post hoc test. * $p < 0.05$, ** $p < 0.01$, *** $p < 0.001$, n.s., not significant. (**E**) Representative images showing toluidine blue-stained, semi-thin cross-sections of sciatic nerves dissected from Ctrl or cKO mice at 6 wpi. Scale bars, 10 μm. (**F**–**G**) Quantification of (F) calculated G-ratio values and (G) axon diameters from analyzing toluidine blue-stained sciatic nerve sections dissected from Ctrl or cKO mice at 6 wpi. 50 axons were randomly selected from each sciatic nerve for quantification. n = 5. Mann-Whitney U test. *** $p < 0.001$, n.s., not significant.

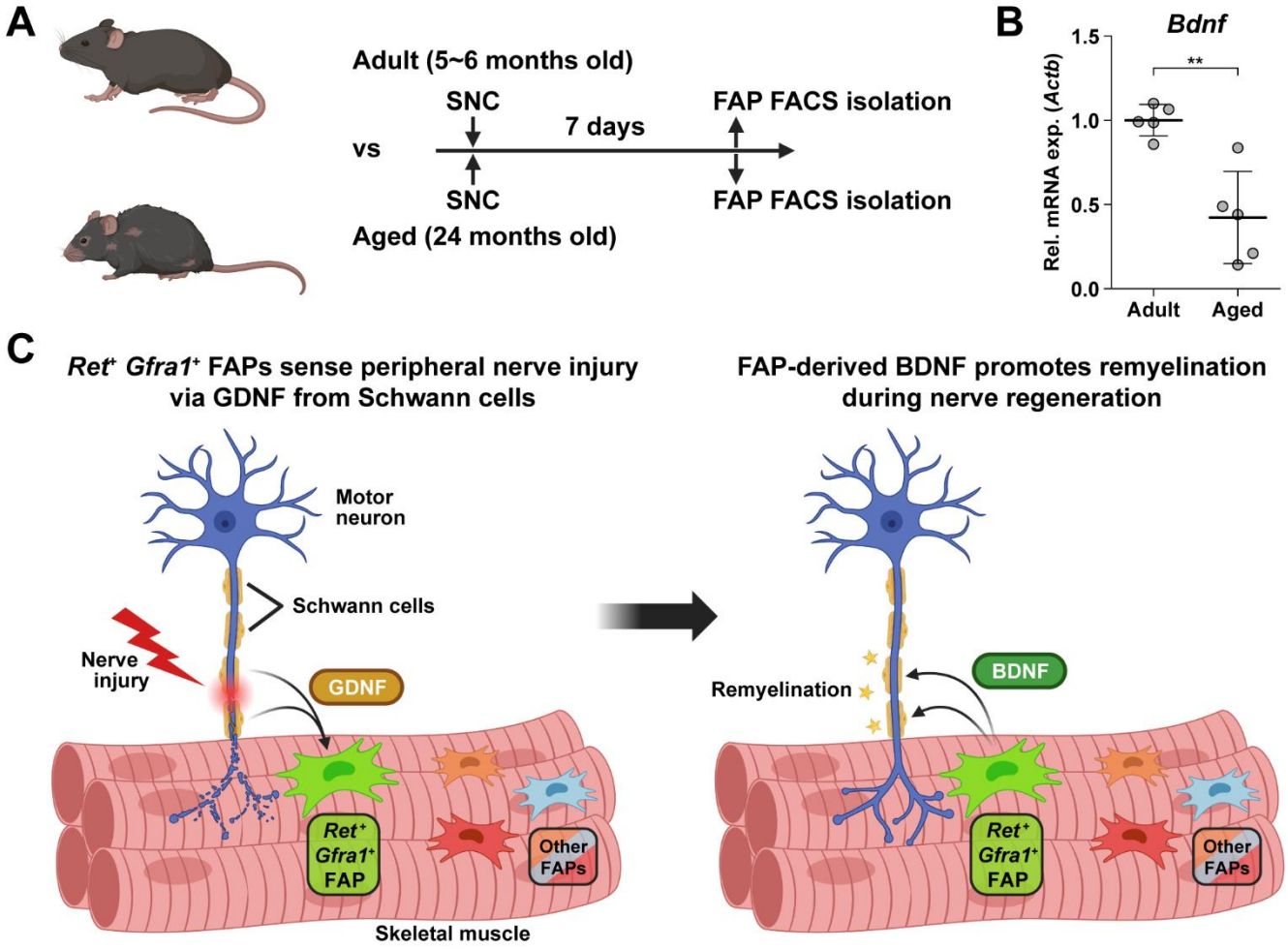


**Figure 6. Implication of FAP-derived BDNF in the age-related delay in nerve regeneration.**
(**A**) Experimental scheme indicating ages of mice used and the time point for FAP isolation to compare the expression level of *Bdnf* post SNC. (**B**) RT-qPCR results showing the expression level of *Bdnf* in FAPs isolated from either adult (5-6 months) or aged (24 months) mice at 7 dpi. n = 5. Unpaired t-test. ** $p < 0.01$. (**C**) Graphical summary of this study.

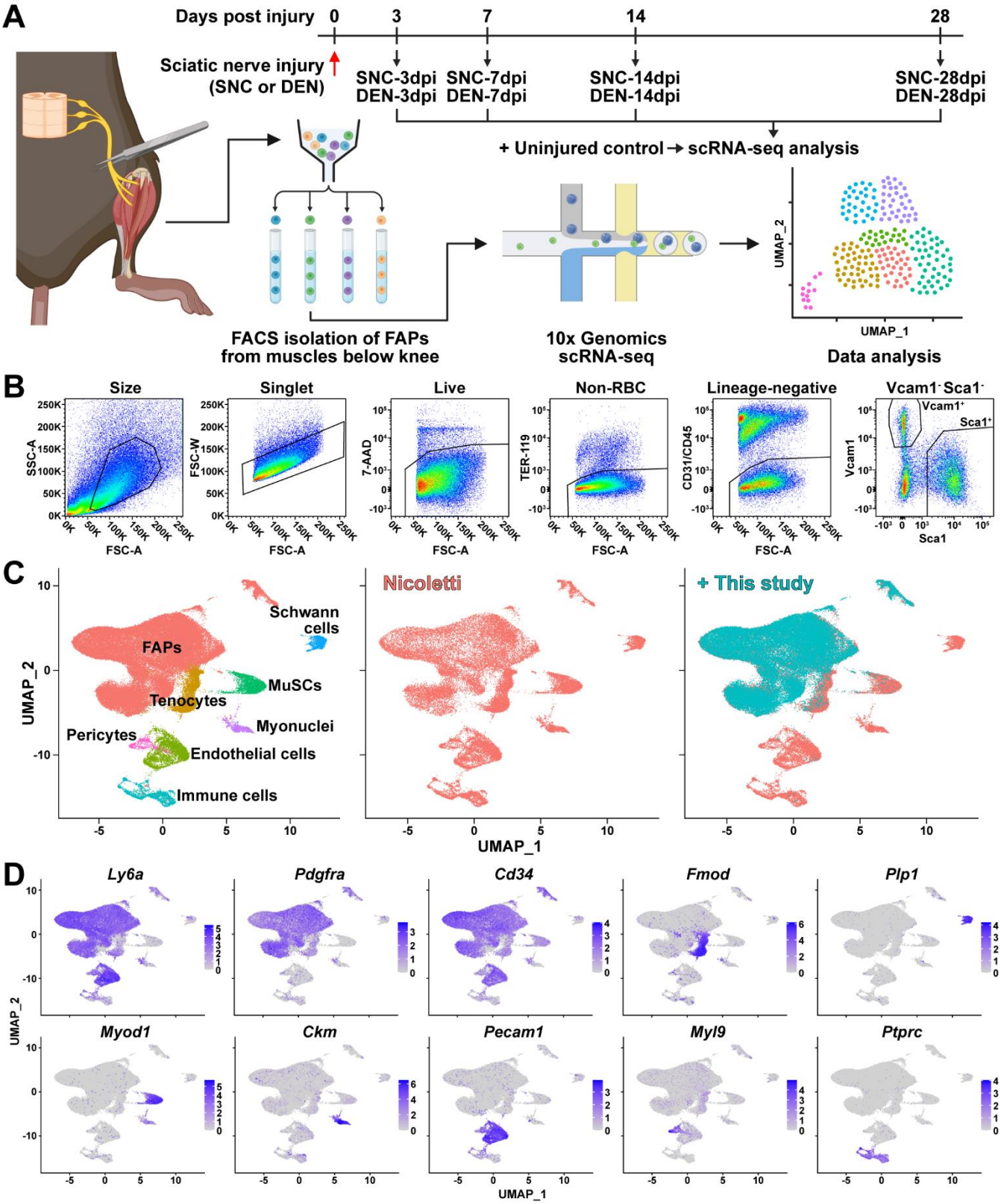


**Figure 1—figure supplement 1. Establishment and validation of nerve injury-affected FAPs' scRNA-seq data.**

(**A**) Experimental scheme depicting the procedures for sample collection and scRNA-seq. The types of nerve injuries and time points for FAP isolation for each sample are specified. (**B**) Gating strategies used for FACS isolation of FAPs. (**C**) Integration of scRNA-seq data obtained in this study and data from Nicoletti et al. (2023) visualized on UMAP plots. Left: integrated data labeled with cell types; middle: cells from Nicoletti et al. (2023) only; right: data from this study overlaid on top of data from Nicoletti et al. (2023). (**D**) Expressions of marker genes that distinguish cell types within skeletal muscle in the integrated scRNA-seq data visualized on UMAP plots.

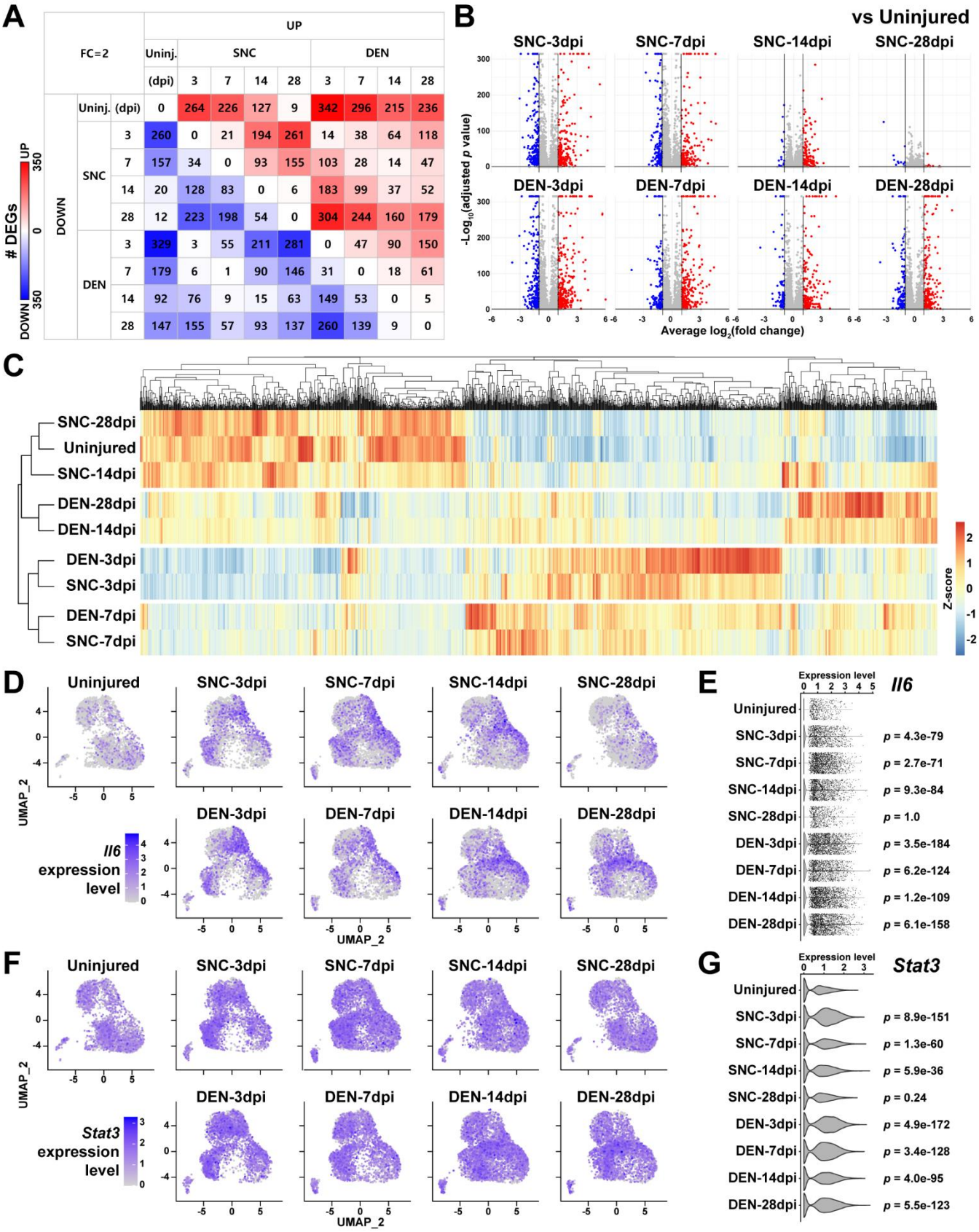


**Figure 1—figure supplement 2. DEG analyses reveal similarities and differences between FAPs affected by SNC or DEN at different time points.**

(**A**) Number of DEGs identified from pairwise comparisons of all nine scRNA-seq samples visualized as a heatmap. (**B**) DEGs identified from comparing nerve injury-affected FAPs versus uninjured control shown on volcano plots. (**C**) Hierarchical clustering of the nine scRNA-seq samples using DEGs identified in (A) displayed as a heatmap. (**D** and **F**) UMAP plots showing the expressions of (D) *Il6* and (F) *Stat3*. (**E** and **G**) Violin plots showing the expressions of (E) *Il6* and (G) *Stat3*, with p values calculated from comparing each sample to uninjured control. Wilcoxon rank sum test.

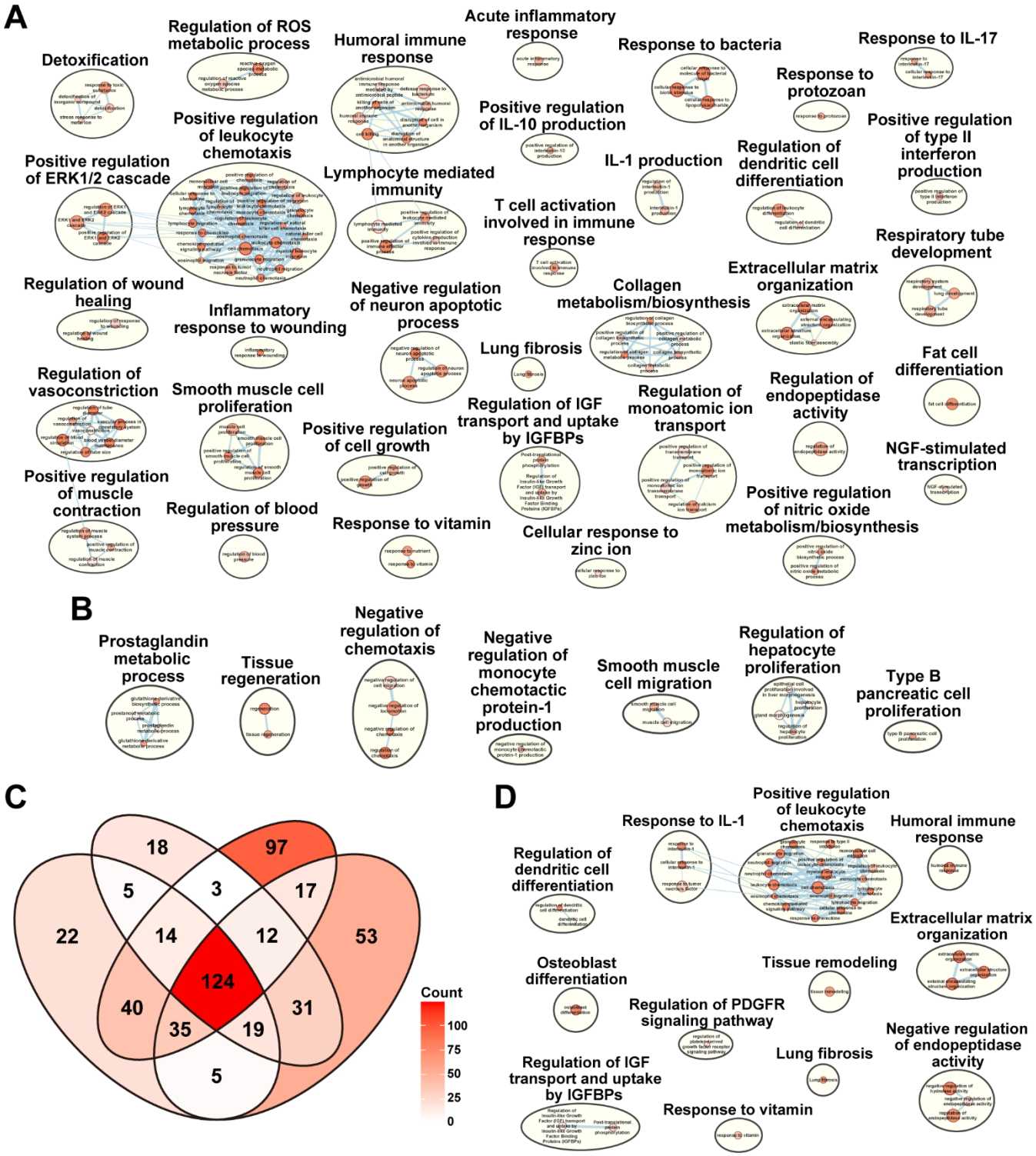


**Figure 1—figure supplement 3. Gene set overrepresentation analyses using DEGs from pairwise comparisons of the nine scRNA-seq samples.**

(**A**–**B**) Results from g:Profiler showing pathways enriched using DEGs upregulated in (A) DEN-28dpi versus SNC-28dpi and (B) vice versa. (**C**) Venn diagram showing the number of overlapping genes identified as DEGs by comparing each indicated sample to uninjured control. (**D**) Results from g:Profiler showing pathways enriched using DEGs shared in all four samples compared to uninjured control, as shown in (C).

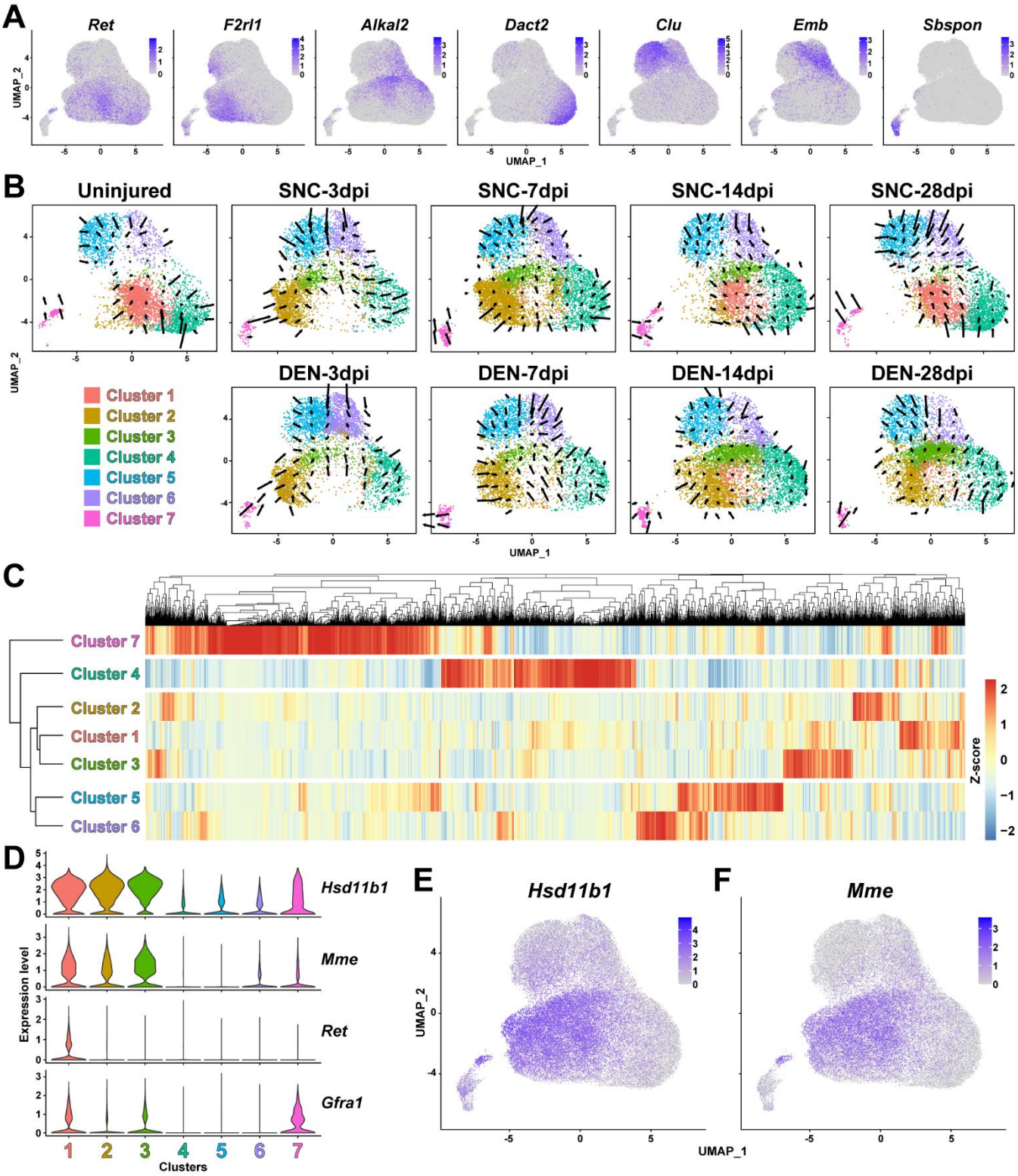


**Figure 2—figure supplement 1. Identification of FAP clusters that respond to nerve injury.**
(**A**) UMAP plots showing expressions of cluster-specific marker genes identified in this study. (**B**) Results from RNA velocity analysis visualized on UMAP plots. Arrows indicate the predicted direction of cellular movement in the near future on the UMAP plots. (**C**) Hierarchical clustering of the seven FAP clusters displayed with a heatmap. (**D**) Violin plots showing the expressions of marker genes previously reported by Leinroth et al. (2022) in the seven clusters identified in this study. (**E**–**F**) Expressions of (E) *Hsd11b1* and (F) *Mme* shown on UMAP plots.

**A**

| Gene | Average $\log_2$FC | Adjusted *p* value |
|---|---|---|
| *Ret* | 2.266 | $<10^{-303}$ |
| *Ifi30* | 1.706 | |
| *Prss12* | 1.665 | |
| *Col5a3* | 1.573 | |
| *Atp1a2* | 1.543 | |
| *Col6a6* | 1.455 | |
| *G0s2* | 1.451 | |
| *Enpp2* | 1.427 | |
| *Nmb* | 1.412 | |
| *Gfra1* | 1.395 | |

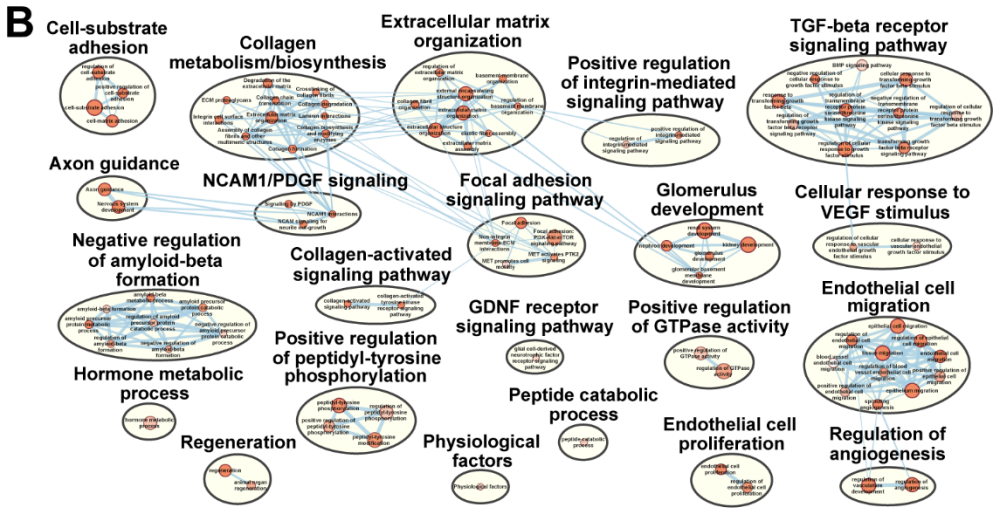


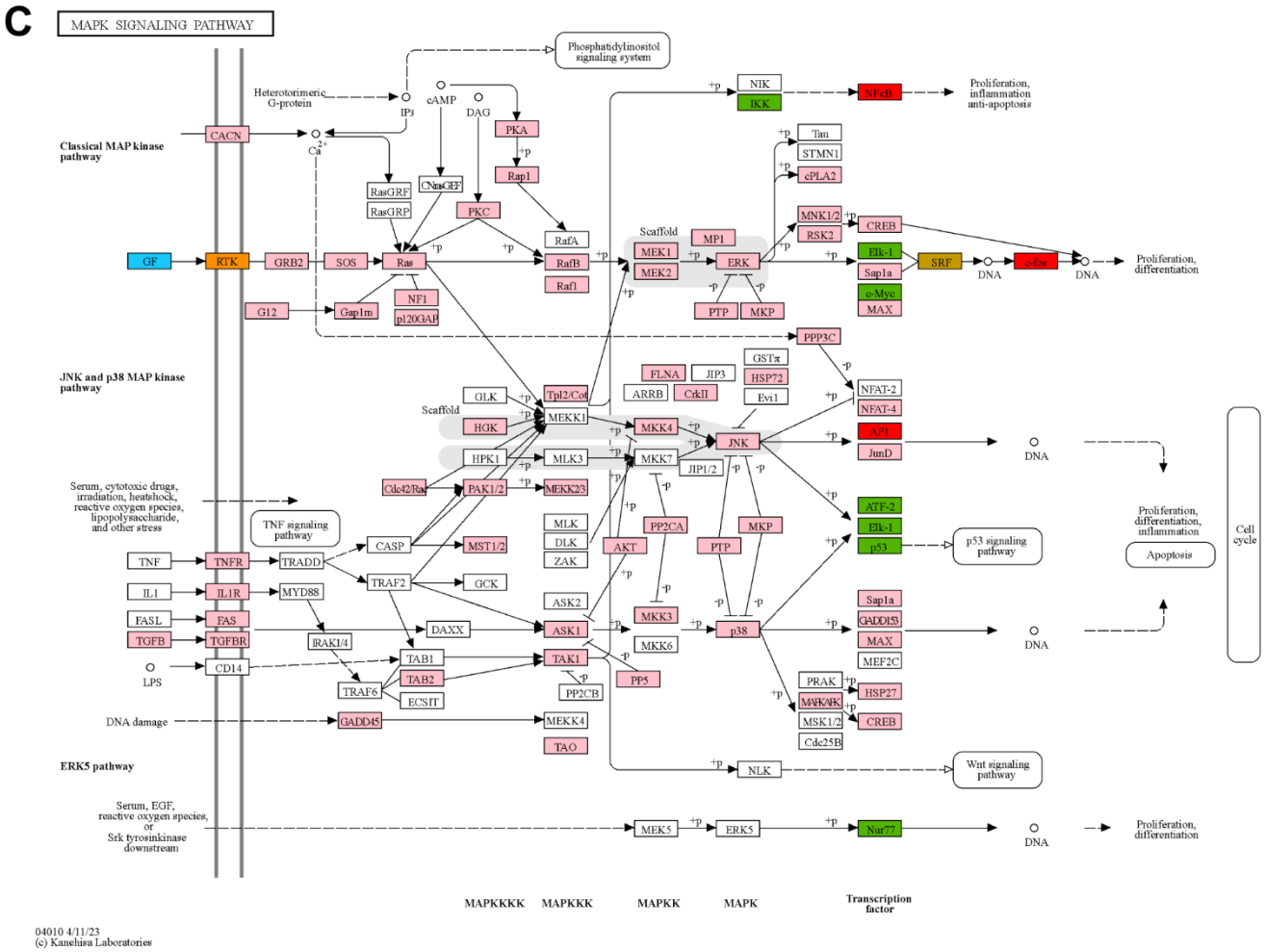


**Figure 3—figure supplement 1. Involvement of GDNF signaling pathway in the nerve injury-sensing mechanism by cluster 1 FAPs.**

(**A**) Top 10 genes specifically enriched in cluster 1 FAPs. P values were drawn from Wilcoxon rank sum test. (**B**) Results from g:Profiler showing pathways enriched using genes specifically enriched in cluster 1. (**C**) MAPK signaling pathway retrieved from KEGG, with color-coding to highlight relevant genes. Blue: GDNF ligand; orange: GDNF receptor Ret expressed in cluster 1; pink: downstream cascade genes expressed in clusters 1-3; red: transcription factors (TFs) commonly predicted to regulate upregulated genes in clusters 2 and 3; green: TFs predicted to regulate genes upregulated in cluster 2; gold: TFs predicted to regulate genes upregulated in cluster 3.

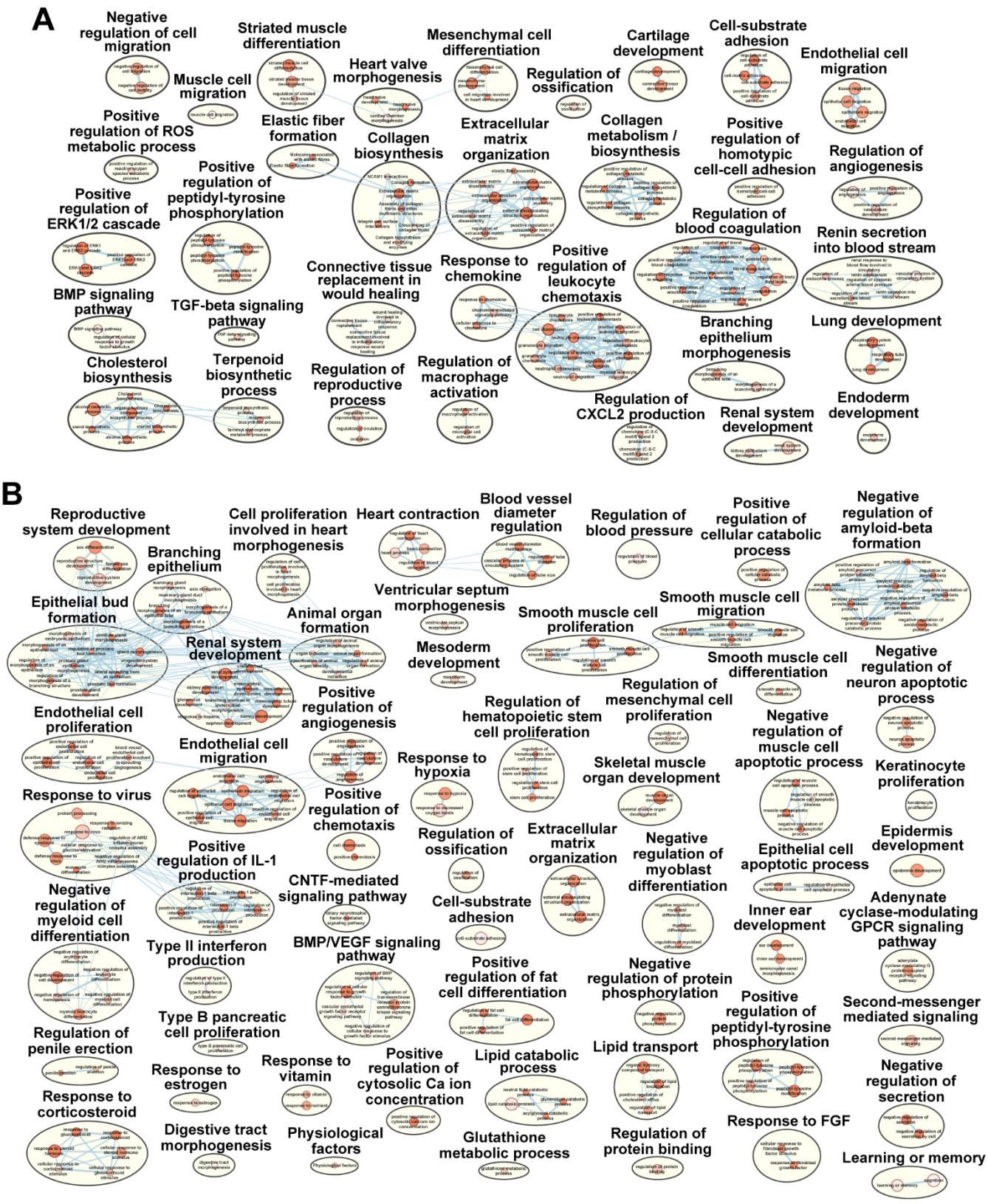


**Figure 3—figure supplement 2. Pathways enriched in the two activated clusters within nerve injury-affected FAPs.**

(**A**–**B**) Results from g:Profiler showing pathways enriched using genes specifically enriched in (A) cluster 2 or (B) cluster 3.

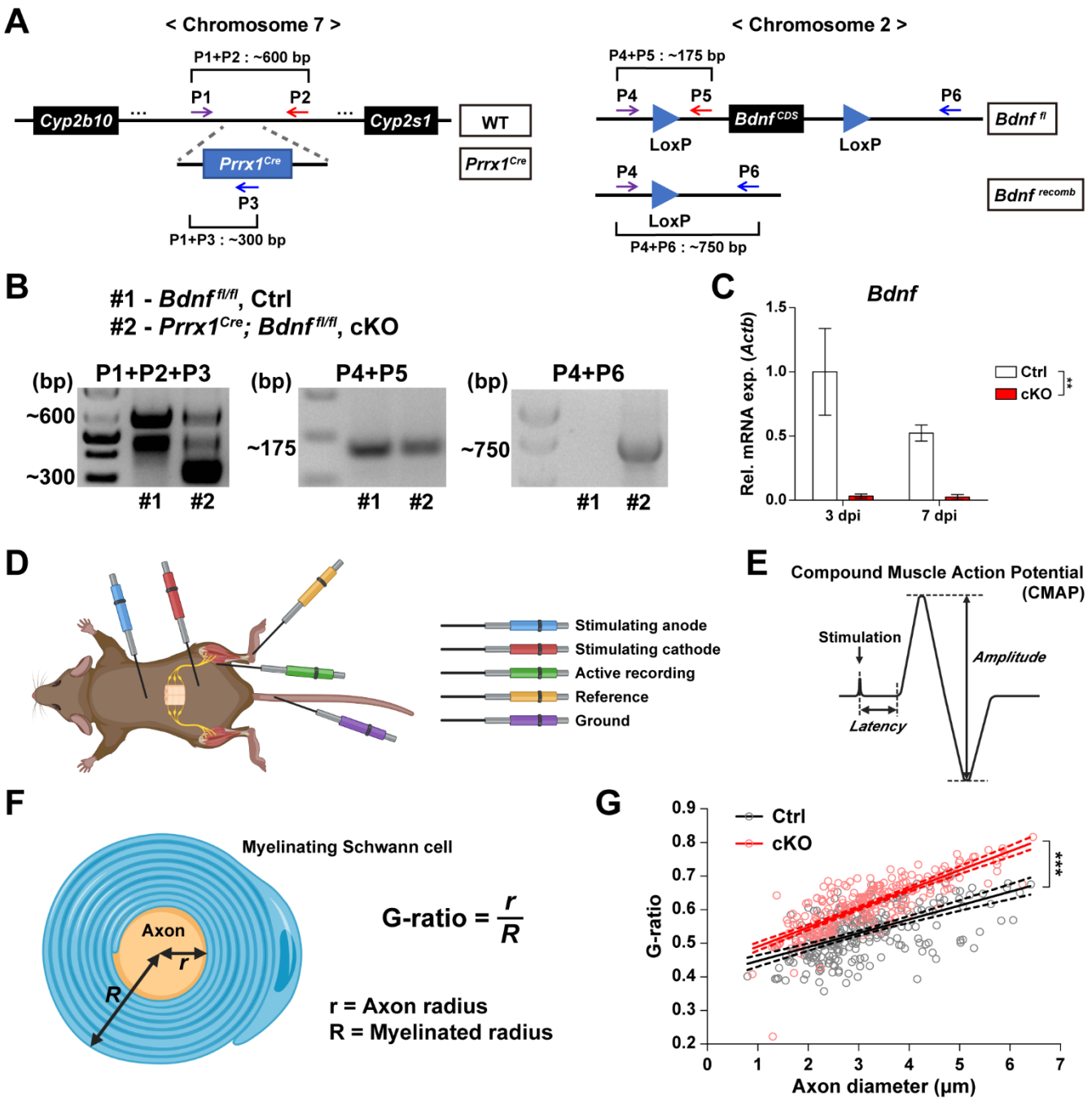


**Figure 5—figure supplement 1. Validation of cKO mice used in this study and methods used for analysis.** (**A**) Genomic loci and structure of *Prrx1*$^{Cre}$ and *Bdnf*$^{fl}$ alleles labeled with primers used for genotyping and genomic DNA recombination validation. (**B**) Results from genotyping (left and middle) and genomic DNA recombination PCR (right). Genomic DNA recombination of the LoxP flanking sites in the cKO mice were confirmed using primers P4 and P6 shown in (A). (**C**) RT-qPCR results of *Bdnf* expression using FAPs isolated from either Ctrl or cKO mice at 3 or 7 days post SNC. n = 2; Two-way ANOVA. ** $p < 0.01$. (**D**) Scheme for CMAP measurement showing the positions of electrodes used. (**E**) Diagram of a typical CMAP graph along with amplitude and latency used for analysis. (**F**) Diagram depicting calculation of G-ratio. (**G**) Scatter plots with linear regressions displaying G-ratios (y-axis) in relation to axon diameters (x-axis). Solid lines are linear regressions and dotted lines represent error in 95% confidence level. ANCOVA, *** $p < 0.001$.

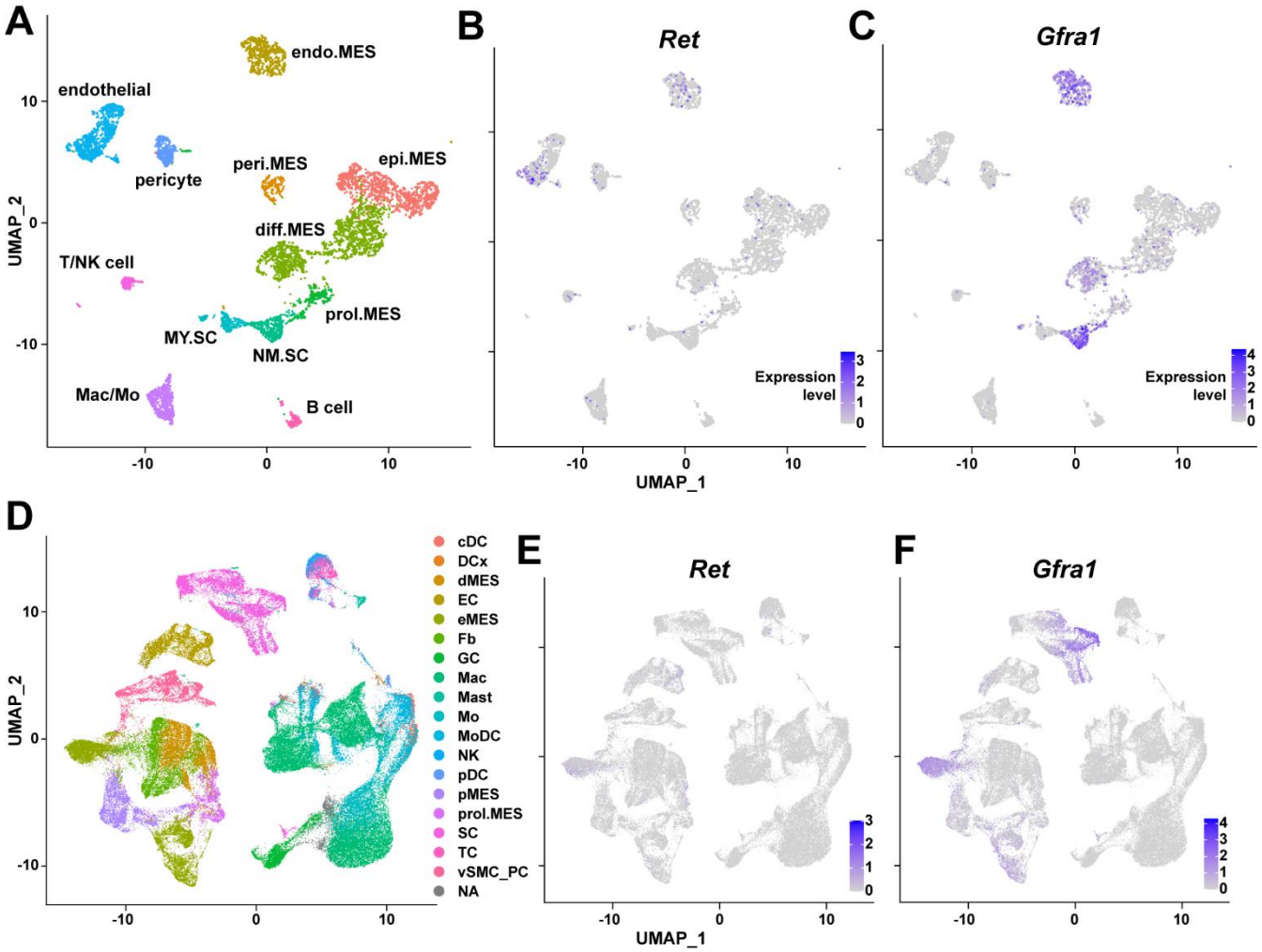


**Supplemental figure 1. Expression of GDNF receptor genes *Ret* and *Gfra1* in nerve-resident cells.** (**A**–**C**) scRNA-seq data from Carr et al. (2019) and Toma et al. (2020) (accession numbers: GSM3408137, GSM3408139, GSM4423509, GSM4423506) were merged into a single Seurat object and visualized on UMAP plots. Cell types identified using markers listed by Toma et al. (2020) are shown in (A), and expression levels of (B) *Ret* and (C) *Gfra1* are displayed. epi.MES: epineurial mesenchymal cells; peri.MES: perineurial mesenchymal cells; endo.MES: endoneurial mesenchymal cells; diff.MES: differentiating mesenchymal cells; prol.MES: proliferating mesenchymal cells; NM.SC: non-myelinating Schwann cells; MY.SC: myelinating Schwann cells; Mac/Mo: macrophage/monocyte. (**D**–**F**) scRNA-seq data from Zhao et al. (2022) (accession number: GSE198582) were merged into a single Seurat object and visualized on UMAP plots. Cell types annotated by Zhao et al. (2022) are shown in (D), and expression levels of (E) *Ret* and (F) *Gfra1* are displayed. cDC: conventional dendritic cells; DCx: dendritic cells destined for homing; dMES: differentiating mesenchymal cells; EC: endothelial cells; eMES: endoneurial mesenchymal cells; Fb: fibroblasts; GC: granulocytes; Mac: macrophages; Mast: mast cells; Mo: monocytes; MoDC: monocyte-derived dendritic cells; NK: natural killer cells; pDC: plasmocytoid dendritic cells; pMES: perineurial mesenchymal cells; prol.MES: proliferating mesenchymal cells; SC: Schwann cells; TC: T cells; vSMC_PC: vascular smooth muscle cells/pericytes; NA: not applicable.

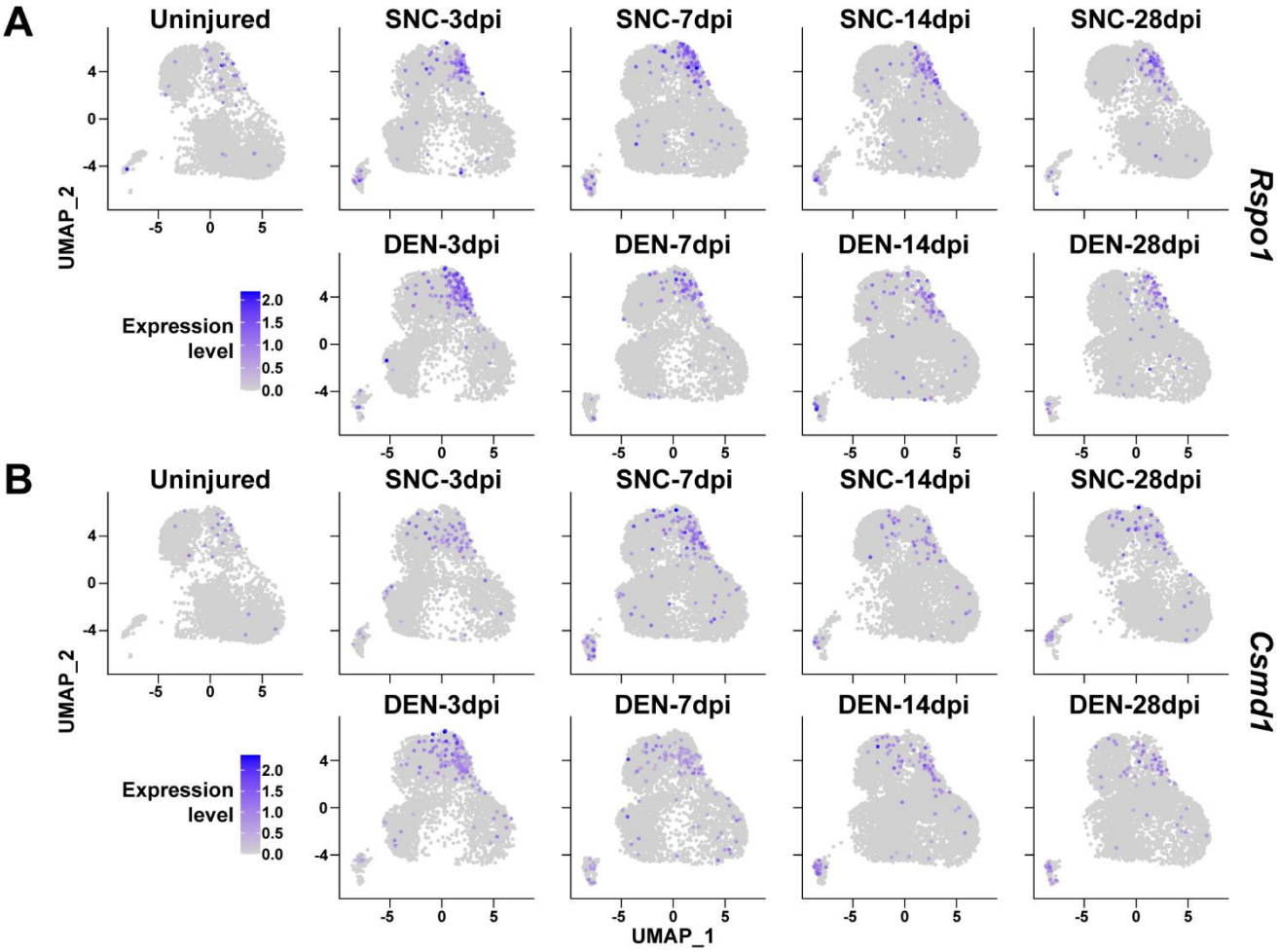


**Supplemental figure 2. Expression of nerve injury-induced, cluster-specific genes in FAPs.**
(**A**–**B**) Expressions of (A) *Rspo1* and (B) *Csmd1* shown on UMAP plots, separated by samples. scRNA-seq data obtained in this study were used.

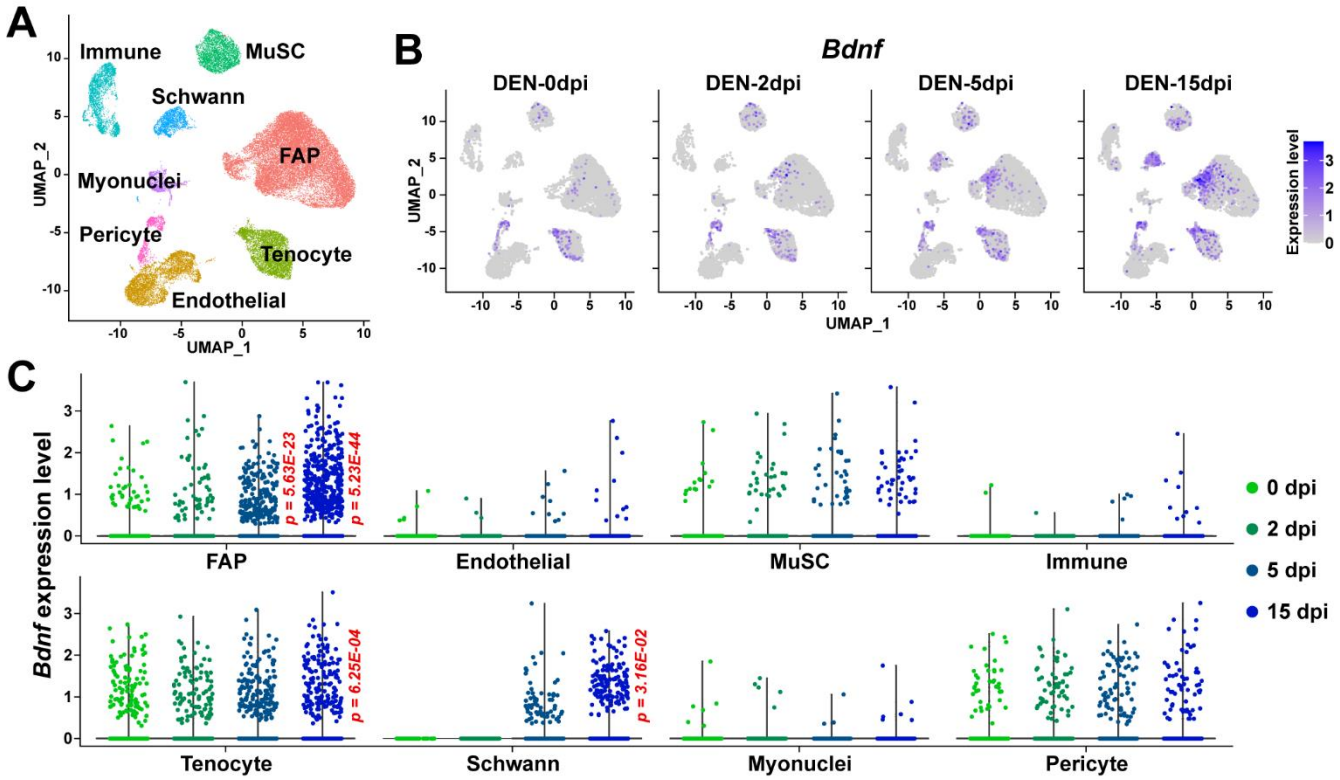


**Supplemental figure 3. Expression of *Bdnf* in muscle-resident mononuclear cells affected by denervation.** (**A**) UMAP plot showing data from Nicoletti et al. (2023) labeled by cell types identified. (**B**) Expression pattern of *Bdnf* in data from Nicoletti et al. (2023) shown on UMAP plots, separately by days post denervation. (**C**) Expression of *Bdnf* in each cell type on different days post denervation displayed in violin plots. P values were calculated by comparing each injury-affected cells' expression levels versus its uninjured state (0 dpi). Only significant p values are shown. Wilcoxon rank sum test.

**Supplemental table 1. Results from TRRUST showing transcription factors predicted to regulate genes specifically enriched in cluster 2.** Genes known to be regulated by each transcription factor is listed.

| Key TF | Adjusted P value | List of overlapped genes |
|---|---|---|
| Jun | 0.000114 | Timp1, C1qtnf3, Plaur, Slc39a14, Mmp3, Itga5, Serpine1, Tgfb1, Mmp19, Ccl2, Slc8a1, Plau |
| Smad3 | 0.000399 | Serpine1, Plau, Nedd9, Acta2, Ccl2, Tagln, Enpp1 |
| Msx2 | 0.00464 | Lss, Enpp1, Tagln, Alpl |
| Smad1 | 0.00579 | Runx1, Col4a1, Col4a2, Tnfrsf11b |
| Ppard | 0.00579 | Angptl4, Tgfb1, Insig1 |
| Sp1 | 0.00579 | Acta2, Trf, Serpine1, Plaur, Lgals1, Mgp, Ccl2, Nes, Adcyap1r1, Itga5, Bmp4, Notch1, Skil |
| Fos | 0.0149 | Tgfb1, Bdnf, Tslp, Plau, Pdpn |
| Tgfb1i1 | 0.0149 | Ccl2, Tgfb1 |
| Srf | 0.0185 | Tagln, Barx2, Acta2 |
| Id3 | 0.0298 | Notch1, Alpl |
| Nfkb1 | 0.0298 | Mmp3, Tgfb1, Dmp1, Pla2g4a, Il15, Egr2, Plaur, Ppp1r13l, Ccl2 |
| Junb | 0.034 | Plau, Serpine1 |
| Pparg | 0.034 | Serpine1, Muc1, Angptl4, C1qtnf3 |
| Nfkb2 | 0.0362 | Hif1a, Dmp1 |
| Id1 | 0.0382 | Thbs1, Alpl |
| Runx2 | 0.0382 | Alpl, Mgp, Thbs1, Enpp1 |
| Arntl | 0.0382 | Cxcl5, Bhlhe41 |
| Msx1 | 0.0382 | Tagln, Bmp4 |
| Nr4a2 | 0.0382 | Tnc, Gch1 |
| Ets1 | 0.0388 | Timp1, Mmp3, Ccl2, Bmp4 |
| Prox1 | 0.0465 | Pdpn, Notch1 |
| Bcl3 | 0.0465 | Runx1, Tnfrsf12a |
| Clock | 0.0465 | Serpine1, Bhlhe41 |
| Etv4 | 0.0465 | Mmp3, Plau |

**Supplemental table 2. Results from TRRUST showing transcription factors predicted to regulate genes specifically enriched in cluster 3.** Genes known to be regulated by each transcription factor is listed.

| Key TF | Adjusted P value | List of overlapped genes |
|---|---|---|
| Nfkb1 | 1.64E-05 | Cxcl10, Tnfsf13b, Cebpa, Apoe, Cxcl1, Il12a, Myc, Vcam1, Tnf, Sox9, Plin2, Rel, Igf2bp2, Birc3, Hmox1, Nfkbiz, Bcl2 |
| Cebpb | 0.000206 | Bcl2, Myc, Mafb, Cebpa, Btg2, Serpine1, Socs3 |
| Sp1 | 0.000206 | Ces1d, Myc, Mgarp, Serpine1, Sirt1, Cebpd, Egr1, Apoe, Cebpa, Slc2a3, Socs3, Adcyap1r1, Tnf, Ar, Lpl, Bmp4, Igfbp3 |
| Dlx5 | 0.000206 | Wnt5a, Alpl, Myc, Igfbp3 |
| Stat3 | 0.000206 | Mt1, Il12a, Pnp, Socs3, Bcl2, Cebpd, Egr1, Tnf, Myc |
| Rela | 0.000206 | Tnfsf13b, Myc, Vcam1, Igf2bp2, Birc3, Pgf, Sox9, Cxcl10, Apoe, Tnf, Bcl2 |
| Stat1 | 0.000336 | Cxcl9, Egr1, Mt1, Socs3, Cebpd, Cxcl10 |
| Id1 | 0.000336 | Thbs1, Alpl, Rel, Tnf |
| Crebbp | 0.000876 | Socs3, Fosb, Tnf, Hmox1, Bcl2, Mt1 |
| Rel | 0.00115 | Cebpd, Birc3, Il12a, Tnf, Myc |
| Jun | 0.00119 | Plin2, Cebpd, Cxcl1, Serpine1, Hmox1, Aldh1a1, Tnf, Sirt1, Socs3, Plau |
| Hnf1b | 0.00135 | Mafb, Pde4c, Socs3 |
| Hif1a | 0.00324 | Mt1, Cited2, Hmox1, Serpine1 |
| Tfap2a | 0.00381 | Apoe, Cebpa, Meis1 |
| Trp53 | 0.00595 | Btg2, Thbs1, Hmox1, Bcl2, Mt1, Agtr1a, Myc, Serpine1, Egr1, Pappa |
| Ikbkb | 0.00595 | Cxcl9, Cxcl10, Tnf |
| Epas1 | 0.00678 | Serpine1, Cited2, Vcam1 |
| Ppara | 0.00678 | Cebpa, Lpl, Cebpd, Serpine1, Bcl2 |
| Twist1 | 0.00781 | Fgf10, Sox9, Tnf, Mme |
| Smad3 | 0.00809 | Serpine1, Plau, Sirt1, Tnfsf13b, Myc |
| Bcl3 | 0.00899 | Tnf, Cxcl10, Ubc |
| Atf2 | 0.0104 | Sox9, Cebpa, Tnf |
| Fos | 0.0127 | Socs3, Tslp, Mt1, Plau, Egr1 |
| Etv2 | 0.0146 | Sox9, Plau |
| Mtf1 | 0.0146 | Pgf, Mt1 |
| Rbl1 | 0.0146 | Myc, Alpl |
| Ctnnb1 | 0.0167 | Bmp4, Isl1, Myc, Tbx3, Gja1 |
| Elk1 | 0.0181 | Hmox1, Egr1 |
| Fosl1 | 0.0181 | Thbs1, Thbs2 |
| Dnmt3a | 0.0209 | Vtn, Mt1 |
| Foxg1 | 0.0209 | Ebf3, Serpine1 |
| Id3 | 0.0209 | Vcam1, Alpl |
| Tbx1 | 0.0209 | Ripply3, Fgf10 |
| Egr1 | 0.0225 | Tnf, Serpine1, Thbs1, Nr4a1, Il12a |
| Irf1 | 0.0225 | Cxcl10, Il12a, Tnf |
| Foxo3 | 0.0225 | Socs3, Sirt1 |
| Gfi1b | 0.0225 | Meis1, Socs3 |
| Junb | 0.0225 | Plau, Serpine1 |
| Ncoa3 | 0.0225 | Igfbp3, Tbx3 |
| Foxo1 | 0.0242 | Bcl2l11, Egr1, Lpl, Alpl |

*(Continued)*

| | | |
|---|---|---|
| Myc | 0.0242 | Myc, Cebpd, Bcl2, Zfp36 |
| Pparg | 0.0246 | Serpine1, Plin2, Egr1, Hmox1 |
| Nfkb2 | 0.0246 | Myc, Rel |
| Nr4a1 | 0.0246 | Serpine1, Ar |
| Nfe2l2 | 0.0278 | Bcl2, Hmox1, Sult1e1, Mt1 |
| Id2 | 0.0278 | Alpl, Zbtb16 |
| Klf5 | 0.0278 | Egr1, Serpine1 |
| Creb1 | 0.0312 | Bcl2, Nfkbiz, Slc2a3 |
| Runx2 | 0.0336 | Alpl, Thbs1, Hbegf, Sox9 |
| Ets1 | 0.0369 | Egr1, Hmox1, Nr2f1, Bmp4 |
| Ep300 | 0.0382 | Tnfsf13b, Mt1, Hmox1, Socs3 |
| Usf2 | 0.04 | Hmox1, Mt1 |
| Mecp2 | 0.0496 | Slc2a3, Igfbp3 |
| Stat6 | 0.0496 | Tnf, Egr1 |

**Supplemental table 3. Categorization of genes predicted to be regulated by transcription factors that act downstream of the GDNF signaling pathway.** Note that only *Bdnf* fits into all three criteria.

| Gene | Secreted | GO term related to neuron/glial cell regulation | Exclusive expression in activated FAPs |
|---|---|---|---|
| Bdnf | O | O | O |
| Apoe | O | O | X |
| Ccl2 | O | O | X |
| Tgfb1 | O | O | X |
| Tnf | O | O | X |
| Vcam1 | O | O | X |
| Dmp1 | O | X | O |
| C1qtnf3 | O | X | X |
| Cxcl1 | O | X | X |
| Cxcl10 | O | X | X |
| Il12a | O | X | X |
| Il15 | O | X | X |
| Mmp19 | O | X | X |
| Mmp3 | O | X | X |
| Plau | O | X | X |
| Plaur | O | X | X |
| Serpine1 | O | X | X |
| Timp1 | O | X | X |
| Tnfsf13b | O | X | X |
| Tslp | O | X | X |
| Bcl2 | X | O | X |
| Egr1 | X | O | X |
| Egr2 | X | O | X |
| Hif1a | X | O | X |
| Hmox1 | X | O | X |
| Igf2bp2 | X | O | X |
| Mt1 | X | O | X |
| Myc | X | O | X |
| Rel | X | O | X |
| Sirt1 | X | O | X |
| Sox9 | X | O | X |
| Aldh1a1 | X | X | X |
| Birc3 | X | X | X |
| Cebpa | X | X | X |
| Cebpd | X | X | X |
| Itga5 | X | X | X |
| Nfkbiz | X | X | X |
| Pdpn | X | X | X |
| Pla2g4a | X | X | X |
| Plin2 | X | X | X |
| Ppp1r13l | X | X | X |
| Slc39a14 | X | X | X |
| Slc8a1 | X | X | X |
| Socs3 | X | X | X |

**Supplemental table 4. Primers used in this study for genotyping PCR or RT-qPCR.**

| No. | Primer | Usage | Sequence (5' to 3') |
|---|---|---|---|
| 1 | Prrx1Cre_com_R (P1) | Genotyping PCR | TAG TGA AGT GGA AGT TCC TGG |
| 2 | Prrx1Cre_WT_F (P2) | Genotyping PCR | CAG TTC CTA CCC TGA TTT CC |
| 3 | Prrx1Cre_Tg_F (P3) | Genotyping PCR | GAT CAT AAT CAG CCA TAC CAC |
| 4 | Bdnf_flox_F (P4) | Genotyping PCR | TGT GAT TGT GTT TCT GGT GAC |
| 5 | Bdnf_flox_R (P5) | Genotyping PCR | CGG TTT CTA AGC AAG TGA ACA |
| 6 | Bdnf_recomb_R (P6) | Genotyping PCR | GAA ATT TTC TCC ATC CCT ACT CCG GG |
| 7 | Cre_F | Genotyping PCR | GCA TTA CCG GTC GAT GCA ACG AGT GAT GAG |
| 8 | Cre_R | Genotyping PCR | GAG TGA ACG AAC CTG GTC GAA ATC AGT GCG |
| 9 | Rosa-tdT_WT_F | Genotyping PCR | AAG GGA GCT GCA GTG GAG TA |
| 10 | Rosa-tdT_WT_R | Genotyping PCR | CCG AAA ATC TGT GGG AAG TC |
| 11 | Rosa-tdT_Tg_F | Genotyping PCR | GGC ATT AAA GCA GCG TAT CC |
| 12 | Rosa-tdT_Tg_R | Genotyping PCR | CTG TTC CTG TAC GGC ATG G |
| 13 | Actb_qF | RT-qPCR | CCT CCC TGG AGA AGA GCT ATG |
| 14 | Actb_qR | RT-qPCR | TTA CGG ATG TCA ACG TCA CAC |
| 15 | Ret_qF | RT-qPCR | CCA GGG CTT CCC AAT CAG TT |
| 16 | Ret_qR | RT-qPCR | TTC CAA ACT CGC CTT CTC CC |
| 17 | Gfra1_qF | RT-qPCR | CAC TCC TGG ATT TGC TGA TGT |
| 18 | Gfra1_qR | RT-qPCR | AGT GTG CGG TAC TTG GTG C |
| 19 | Gdnf_qF | RT-qPCR | TCG GCC GAG ACA ATG TAT GA |
| 20 | Gdnf_qR | RT-qPCR | CAA CAT GCC TGG CCT ACT TTG |
| 21 | Bdnf_qF | RT-qPCR | AAG GAC GCG GAC TTG TAC AC |
| 22 | Bdnf_qR | RT-qPCR | CGC TAA TAC TGT CAC ACA CGC |